A new large gomphodont from the Triassic of South Africa and its implications for Gondwanan biostratigraphy

Tolchard, Frederick; Kammerer, Christian; Butler, Richard; Hendrickx, Christophe; Benoit, Julien; Abdala, Fernando; Choiniere, Jonah N.

DOI:
10.1080/02724634.2021.1929265

A new large gomphodont from the Triassic of South Africa and its implications for Gondwanan biostratigraphy

FREDERICK TOLCHARD,[1*] CHRISTIAN F. KAMMERER,[2,5] RICHARD J. BUTLER,[3,5] CHRISTOPHE HENDRICKX,[4,5] JULIEN BENOIT,[5] FERNANDO ABDALA,[4,5] and JONAH N. CHOINIERE[5]

[1] Evolutionary Studies Institute and School of Geosciences, University of the Witwatersrand, Johannesburg, South Africa;

[2] North Carolina Museum of Natural Sciences, 11 W. Jones Street, Raleigh, North Carolina 27601, U.S.A;

[3] School of Geography, Earth and Environmental Sciences, University of Birmingham, Edgbaston, Birmingham B15 2TT, UK;

[4] Unidad Ejecutora Lillo, CONICET-Fundación Miguel Lillo, Miguel Lillo 251, San Miguel de Tucumán 4000, Tucumán, Argentina;

[5] Evolutionary Studies Institute, University of the Witwatersrand, Johannesburg, South Africa

* Corresponding author.

ABSTRACT—A partial skull (BP/1/7976) of a very large cynodont from the Middle Triassic *Cynognathus* Assemblage Zone (*Cricodon-Ufudocyclops* subzone) of South Africa is described. The specimen represents a new gomphodont taxon, *Impidens hancoxi*, gen. sp. nov., diagnosed by five sectorial teeth constituting just over half of the length of the upper postcanine tooth row, and enlarged canine and incisor teeth. BP/1/8123, a skull fragment also from the *Cricodon-Ufudocyclops* subzone, and AMNH FARB 24421, a partial skull from the upper Fremouw Formation of Antarctica, are also referred to the new species. The presence of this taxon in both the upper Fremouw Formation and *Cricodon-Ufudocyclops* subzone strengthens evidence of biostratigraphic correlation between these units. *Impidens hancoxi*, with an inferred skull length of up to 460 mm, was a large-bodied and likely omnivorous gomphodont, and may have played the role of apex predator within the tetrapod fauna of the *Cricodon-Ufudocyclops* subzone.

INTRODUCTION

Gomphodontia is a species-rich clade of Triassic non-mammaliaform cynodonts with a Pangaean distribution. They include the most abundant Triassic cynodonts and were major components of terrestrial ecosystems throughout the Middle and early Late Triassic (Abdala and Ribeiro, 2010; Abdala and Gaetano, 2018). The taxon Gomphodontia was initially established by Seeley (1894) for cynodonts with transversely expanded postcanine teeth bearing complex, multicusped crowns indicative of herbivorous or omnivorous habits. Gomphodontia includes three primary subgroups: Gomphognathidae (usually referred to as Diademodontidae, but see Kammerer et al., [2010] and Hopson [2014]), Trirachodontidae, and Traversodontidae (Liu and Abdala, 2014; Angielczyk and Kammerer, 2018; Hendrickx et al., 2019).

In phylogenetic analyses of gomphodonts, Gomphognathidae is generally recovered as the earliest-diverging subclade, with Trirachodontidae and Traversodontidae forming more deeply-nested sister groups (e.g., Hopson and Kitching, 2001; Liu and Olsen, 2010; Liu and Abdala, 2014; Hendrickx et al., 2020). Gomphognathidae includes the well-known species *Diademodon tetragonus*, which is found in (probable) Middle Triassic strata across Gondwana (Peecook et al., 2018; Wynd et al., 2018), and potentially includes the enigmatic Namibian taxon *Titanogomphodon crassus* (Keyser, 1973; Hendrickx et al., 2019). Traversodontidae is the most species-rich clade of Triassic cynodonts and includes some of the most abundant species of non-mammalian cynodonts, such as *Massetognathus pascuali* and *Scalenodon angustifrons* (Crompton, 1955; Liu and Abdala, 2014; Mancuso et al., 2014; Abdala and Gaetano, 2018; Schmitt et al., 2019; Abdala et al., 2020). Traversodontids were also the latest-surviving group of gomphodonts, with definite records from the Norian (Hopson, 1984; Sues and Olsen, 1990; Sues et al., 1992; Sues et al., 1999; Hopson and Sues, 2006; Gow and Hancox, 1993) and possibly later (Godefroit and Battail, 1997; Godefroit, 1999). Trirachodontidae, known primarily from probable Middle Triassic exposures (Hancox et al., 2020), is comparatively species poor, including only four African taxa currently recognized as valid: *Cricodon metabolus*, *Langbergia modisei*, *Trirachodon berryi*, and *Trirachodon kannemeyeri* (Sidor and Hopson, 2018; although note that this paper refers *T. kannemeyeri* to the genus *Cricodon*). The Chinese Sinognathinae (*Beishanodon* and *Sinognathus*) have usually also been included in Trirachodontidae (e.g., Gao et al., 2010; Liu and Abdala, 2014; Hendrickx et al., 2020), although Sidor and Hopson (2018) recovered them as basal traversodontids in their phylogenetic analysis. The authors of the latter paper also suggested that the sinognathines may be probainognathian cynodonts with phylogenetic affinities to *Aleodon* but were unable to study the specimens of the Chinese taxa firsthand to confirm this (Hopson and Sidor, 2015; Sidor and Hopson, 2018).

Although historically treated as a clade, Hendrickx et al. (2020) recently recovered trirachodontids as a grade at the base of Traversodontidae.

The upper and lower gomphodont (i.e. transversely expanded) postcanines of trirachodontids are characterized by three prominent cusps in a central transverse line, bounded by mesial and distal cingula, which distinguishes them from gomphognathids and traversodontids (Abdala et al., 2006; Hendrickx et al., 2019). In known trirachodontids, the postcanine tooth row is mostly composed of these molariform gomphodont teeth (7–10 tooth positions), with only a few (1–3) sectorial teeth at the back of the tooth row. Such complex, transversely-expanded cheek teeth are usually considered indicative of high-fiber herbivory (e.g., Reisz and Sues, 2000). Sectorial teeth are indicative of carnivory, and the retention of sectorials along with gomphodont teeth in trirachodontids suggests that the group may have been omnivorous. Gow (1978) suggested trirachodontids were carnivorous on the basis of their serrated incisors and canines, and the absence of tooth wear on postcanine crowns. Hendrickx et al. (2020) also suggested that trirachodontids were specialized feeders, but with a diet composed primarily of insects and harder plant material.

Trirachodontid fossils are mainly known from southern Africa, with the majority of specimens found in the Burgersdorp Formation of South Africa (e.g., Abdala et al., 2006; Sidor and Hopson, 2018). The Burgersdorp Formation contains the fossils of the *Cynognathus* Assemblage Zone (AZ), the youngest assemblage zone of the Permo-Triassic Beaufort Group (Kitching, 1995; Hancox et al., 2020). The *Cynognathus* AZ is characterized by the earliest regional records of kannemeyeriiform dicynodonts, an increase in archosauromorph diversity, and the initial radiation of eucynodonts (including gomphodonts). Traditionally, this assemblage zone was considered to range from the latest Early (Olenekian) through the Middle (Anisian) Triassic (Hancox, 2000; Abdala et al., 2005). Recent SHRIMP U-Pb radioisotopic dates for the biostratigraphically-correlated

Puesto Viejo Group in Argentina question that age assessment, instead suggesting a Carnian age (Ottone et al., 2014). However, even more recent CA-TIMS U-Pb dates for another biostratigraphically-correlated unit (the Chinese *Sinokannemeyeria* Fauna) do yield an Anisian age (Liu et al., 2018). Given this conflict, the precise chronostratigraphic attribution of the *Cynognathus* AZ should be considered uncertain, although we favour the traditional (predominantly Middle Triassic) paradigm, as it accords more closely with global stratigraphic ranges for other terrestrial tetrapods.

Historically, the *Cynognathus* AZ was considered to be fairly uniform in composition, with the typical *Cynognathus-Diademodon-Kannemeyeria* fauna represented throughout its span (Broom, 1907; Kitching, 1977; Keyser, 1979). However, Hancox et al. (1995) determined that this faunal association only characterizes the middle section of the Burgersdorp Formation, and established a threefold subdivision of the *Cynognathus* AZ into the lower *Langbergia-Garjainia*, the middle *Trirachodon-Kannemeyeria*, and the upper *Cricodon-Ufudocyclops* subzones (Hancox et al., 2020). Although these divisions were initially recognized on the basis of temnospondyl amphibian ranges, subsequent research has demonstrated that trirachodontids also show subzone-specific ranges (Abdala et al., 2005, 2006). *Langbergia* is the earliest-appearing African trirachodontid (and gomphodont generally) and is restricted to the *Langbergia-Garjainia* Subzone. Traditional *Trirachodon* (including the species *T. berryi* and *T. kannemeyeri*, the latter considered *Cricodon kannemeyeri* by Sidor and Hopson [2018]) is restricted to the *Trirachodon-Kannemeyeria* Subzone. The youngest and arguably most poorly known portion of the *Cynognathus* AZ, the *Cricodon-Ufudocyclops* Subzone also exhibits a characteristic trirachodontid fauna, although its taxonomic attribution is questionable. Abdala et al., (2005) referred the *Cricodon-Ufudocyclops* Subzone trirachodontids to *Cricodon metabolus*, a species otherwise known from the Manda Beds of Tanzania (Crompton, 1955) and the Ntawere

Formation of Zambia (Sidor and Hopson, 2018). This referral has recently been questioned, however, with Hendrickx et al. (2019) and Kammerer et al. (2019) casting doubt on the attribution of some or all of the *Cricodon-Ufudocyclops* Subzone trirachodontid specimens to *Cricodon*.

Whether or not the *Cricodon-Ufudocyclops* Subzone trirachodontids pertain to *Cricodon* is part of a series of issues problematizing biostratigraphic correlations for this subzone. Hancox and Rubidge (1996; see also Hancox et al., 2013) described *Cricodon-Ufudocyclops* Subzone dicynodont material that they referred to the otherwise-Tanzanian taxon *Angonisaurus*, using this as the basis for correlations with the Lifua Member of the Manda Beds. Shared presence of *Angonisaurus* was also used to correlate the upper Fremouw Formation of Antarctica with the *Cricodon-Ufudocyclops* Subzone and the Manda Beds (Sidor et al., 2014), with the latter then permitting rough correlation with the Omingonde Formation of Namibia and Ntawere Formation of Zambia. However, Kammerer et al. (2019) demonstrated that the South African "*Angonisaurus*" material is referable to a distinct, seemingly endemic taxon (*Ufudocyclops mukanelai*). Furthermore, they argued that the Fremouw Formation "*Angonisaurus*" specimen is identifiable only as an indeterminate stahleckeriid, eliminating the dicynodont-based correlations between the Fremouw Formation, the Manda Beds, and the *Cricodon-Ufudocyclops* Subzone.

A pervasive problem with the biostratigraphic correlation of the *Cricodon-Ufudocyclops* Subzone is the presence of taxa with expansive geographical (e.g., *Diademodon*) and temporal (e.g., *Paracyclotosaurus*) ranges. Currently, the known tetrapod fauna of the *Cricodon-Ufudocyclops* subzone consists of the non-mammaliaform cynodonts *Cynognathus crateronotus*, *Diademodon tetragonus*, an unnamed gomphodont (represented by the specimen BP/1/5538; considered a basal traversodontid by Hendrickx et al. [2020]), and *Cricodon metabolus* (sensu Abdala et al., 2005 and Hendrickx et al., 2020), the

dicynodonts *Shansiodon* sp. (Hancox et al., 2013) and *Ufudocyclops mukanelai* (Kammerer et al., 2019), and the mastodonsaurid temnospondyl amphibian *Paracyclotosaurus morganorum* (Damiani and Hancox, 2003). Of these, only *Cynognathus* and *Diademodon* are definitely present across multiple basins (Wynd et al., 2018), but as these taxa occur broadly through the *Cynognathus* AZ (all three subzones for *Cynognathus*, and the *Trirachodon-Kannemeyeria* and *Cricodon-Ufudocyclops* subzones for *Diademodon*) they are not useful for more precise correlations. The presence of *Shansiodon* suggests similarity with the Chinese *Sinokannemeyeria* Fauna (Anisian; Liu et al., 2018), but specific attribution of the South African specimen is uncertain, hindering precise correlation. It is possible that it represents a distinct, endemic southern African species of *Shansiodon* whose stratigraphic range may not accord with the Chinese species of the genus (Kammerer et al., 2019), similar to the situation of *Paracyclotosaurus morganorum* (a locally endemic species that is part of a globally-distributed genus whose species range from the Early to Middle Triassic; Sidor et al., 2001). *Cricodon metabolus* would then be the only stratigraphically restricted species present in the *Cricodon-Ufudocyclops* Subzone and other basins, but this referral is currently being re-evaluated. Additional fossils from *Cricodon-Ufudocyclops* subzone are clearly needed to clarify the composition of this assemblage and its possible correlation with other Triassic tetrapod faunas.

As part of our ongoing efforts to address these issues, we have been conducting fieldwork in the *Cricodon-Ufudocyclops* Subzone (Bordy et al., 2017; Kammerer et al., 2019). Fieldwork in 2014 recovered the partial rostrum of one of the largest gomphodont cynodonts yet discovered (length of specimen, as preserved, from snout to postorbital area is 315 mm; see Table 1 for other measurements), differing starkly from any previously known member of the clade. Here, we describe this specimen as a new taxon and include it in a phylogenetic analysis. We conclude that the specimen represents an exceptionally large and

possibly predatory trirachodontid. This discovery has interesting implications for the palaeobiology of trirachodontid cynodonts and for the palaeobiogeography of the Gondwanan Middle Triassic.

List of Institutional Abbreviations— AM: Albany Museum, Grahamstown, South Africa; **AMNH FARB**: American Museum of Natural History, Collection of Fossil Amphibians, Reptiles and Birds, New York, New York, USA; **BP**: Evolutionary Studies Institute (formerly Bernard Price Institute for Palaeontological Research), University of the Witwatersrand, Johannesburg, South Africa; **CAPPA/UFSM**: Centro de Apoio à Pesquisa Paleontológica, Universidade Federal de Santa Maria, São João do Polêsine, Brazil; **GSN**: Geological Survey of Namibia, Windhoek, Namibia; **MACN**: Museo Argentino de Ciencias Naturales "Bernardino Rivadavia", Buenos Aires, Argentina; **MCN**: Museu de Ciências Naturais, Fundação Zoobotânica do Rio Grande do Sul, Porto Alegre, Brazil; **MNHN**: Muséum National d'Histoire Naturelle, Paris, France; **NHMUK**: Natural History Museum, London, UK; **NMQR**: National Museum, Bloemfontein, South Africa; **PVL**: Fundación "Miguel Lillo," San Miguel de Tucumán, Argentina; **SAM-PK**: Iziko, the South African Museum, Cape Town, South Africa; **UFRGS**: Universidade Federal do Rio Grande do Sul, Porto Alegre, Brazil; **UMZC**: University Museum of Zoology, Cambridge, UK.

GEOLOGICAL SETTING

BP/1/7976 was found by Michael Day during fieldwork in 2014. The specimen was found on the farm Thala (formerly Buffelskloof) in light greenish-grey, fine-grained sandstone at the same stratigraphic level and within one horizontal meter of BP/1/8208, the holotype of *Ufudocyclops mukanelai* (Kammerer et al., 2019). These specimens are 55 m

above the base of the *Cricodon-Ufudocyclops* Subzone. For detailed geological context for these specimens, refer to Kammerer et al. (2019).

MATERIAL AND METHODS

External Comparative Anatomy

The primary material described here is BP/1/7976. The specimens used for comparison are itemized in Table 2. The dental material was described using the terminology recently proposed by Hendrickx et al. (2019). We estimated the reconstructed basal skull length (BSL) of BP/1/7976 based on the ratio between antorbital length and BSL in other cynognathian cynodonts to produce a range of estimates (detailed in Tables S1 and S2).

Reconstruction of the Maxillary Canal

BP/1/7976 was scanned at the Evolutionary Studies Institute of the University of the Witwatersrand using a Nikon Metrology XTH 225/320 LC (scanning parameters: 140kV, 140µA, detector dimensions 2000 × 2000 × 2000, isotropic voxel size 0.0723mm, 0.5 fps, 1 frame averaging, 2.2 mm copper filter). Three-dimensional rendering of the internal structure of the maxillary canal for the maxillary branch of the trigeminal nerve was conducted using Avizo 9 (FEI VSG, Hillsboro OR, USA; Fire, 1995). The maxillary canal was segmented manually starting from its external (terminal) ends to ensure that only the canals relevant to facial sensitivity and blood supply were selected (i.e. those corresponding to the course of the trigeminal nerve rather than bone trabeculae). Our primary homologies for the rami of the maxillary canals use the corresponding rami of the trigeminal nerve in extant mammals. Note that some vessels and branches of the facial nerve may have shared the canal along with the maxillary nerve (Bellairs, 1949; Düring and Miller, 1979; Witmer,

1995; Abdel-Kader et al., 2011; Leitch and Catania, 2012; see Benoit et al., 2015). Only the maxillary canal for the maxillary branch of the trigeminal nerve is described, as the ophthalmic, nasopalatine, and dentary canals are not preserved. Original scans of the specimen, including all parameters, and .ply surface files of the maxilla and the maxillary branch of the trigeminal nerve are available at the following link: https://www.morphosource.org/projects/000354303?locale=en (the files are currently private but will be opened for download if the paper is accepted).

Phylogenetic Analysis

Impidens hancoxi was included in the phylogenetic character matrix of Sidor and Hopson (2018), a recent phylogenetic analysis of non-mammalian cynodonts. This matrix includes 28 terminals and 78 characters (Appendix S1). All scorings were based on the holotype with the exception of character 44, which was based on the referred specimen BP/1/8123 (Figs. S1 and S2). Two characters from the analysis of Liu and Abdala (2014) were added: character 76 (their character 43) "Postcanine tooth row in adults"; and character 77 (their character 44) "Overall morphology of the upper gomphodont postcanines in occlusive view". One new character (78) was also added: "Maxillary fossa posterior to canine root on lateral snout surface above labial platform". Scorings for all taxa other than *Impidens hancoxi* were taken from the supplemental material of Sidor and Hopson (2018), with the exception of the scorings for trirachodontids for character 57 "Posterior portion maxillary tooth row inset from lateral margin of maxilla (cheek developed)". Previously *Trirachodon berryi*, *Trirachodon kannemeyeri*, and *Cricodon metabolus* were scored as state 2 ("well set in") for this character. However, direct comparisons between trirachodontid specimens and other gomphodonts in the collections of the ESI reveal that the tooth row is less inset in these taxa than in taxa like *Massetognathus pascuali* (BP/1/4245),

and is more comparable to the condition in, e.g., *Pascualgnathus polanskii* (PVL 3466) and *Scalenodon angustifrons* (UMZC T916). As such we have rescored *Trirachodon berryi*, *Trirachodon kannemeyeri*, and *Cricodon metabolus* as state 1 ("moderately set in") matching that of the latter taxa. For character 9 ("Length of secondary palate relative to tooth row") we combined states 1 ("about equal") and 2 ("longer") because we were unable to differentiate between these states. For example, Sidor and Hopson (2018) scored *Probelesodon* as state 1 and *Chiniquodon* as state 2, even though there is extensive overlap in palatal proportions between these taxa (which are frequently considered synonymous; Abdala and Giannini, 2002). For character 59 ("Number of posterior sectorial postcanines") we reworded state 1 from 'three or four' to 'three to five' because there was no state accounting for the existence of a taxon with five sectorial postcanines.

Manipulation of the data matrix was conducted in Mesquite (Maddison and Maddison 2017, Supplementary Data 2). The data matrix was analyzed in TNT (Goloboff and Catalano, 2016) using a traditional search (TBR) with 1000 replications and one MPT saved per replication. A second round of TBR branch swapping was then conducted on the retained MPTs. We *a priori* excluded the problematic taxon Tritylodontidae from our analysis because it has been phylogenetically unstable in recent analyses of cynodonts and because it represents a composite taxon for which scorings can vary across its consistuent members. Additional analyses including this taxon did not alter the position of *Impidens hancoxi* in our topology.

SYSTEMATIC PALAEONTOLOGY

THERAPSIDA Broom, 1905

CYNODONTIA Owen, 1861

EUCYNODONTIA Kemp, 1982

GOMPHODONTIA Seeley, 1894

IMPIDENS gen. nov.

IMPIDENS HANCOXI sp. nov.

(Figs. 1–6B)

Holotype—Right lateroventral portion of a rostrum and partial zygomatic arch and basicranial girder, BP/I/7976 (Figs. 1–6A). The alveoli of the two posteriormost incisor alveoli, canine and complete postcanine series are preserved. The two anteriormost postcanine alveoli preserve teeth with broken crowns.

Referred Specimens—Left maxillary fragment, BP/1/8123, preserving the roots of the canine, PC1 and PC4, and the badly damaged crowns of PC2 and PC3; right partial snout, AMNH FARB 24421 (Fig. 6B), preserving the maxilla, and portions of the premaxilla, jugal, lacrimal, and, possibly, prefrontal.

Horizon and Locality—*Cricodon-Ufudocyclops* Subzone, *Cynognathus* AZ, Beaufort Group, Karoo Basin, South Africa for specimens BP/1/7976 and BP/1/8123. The former specimen was found in coarse green sandstone, on the farm Thala (Buffel's Kuil 11; 31°54.531' S; 26°47.444' E), approximately 3.4 km northwest of Sterkstroom, Inkwanca local municipality, Chris Hani district municipality, Eastern Cape province, South Africa. The specimen BP/1/8123 was recovered as surface float at the same locality during the same fieldtrip. The specimen AMNH FARB 24421, discovered during a 1985−1986 field trip by Dr William R. Hammer, was found in the upper Fremouw Formation of the Gordon Valley, Beardmore Glacier region of the Transantarctic Mountains, Antarctica (Hammer, 1995).

Diagnosis—Very large gomphodont cynodont (estimated skull length > 400 mm; Table S1 and S2) characterized by enlarged upper incisor (mesiodistal dimensions of I4 alveolus 11.76% of secondary palate length) and canine teeth (mesiodistal dimensions 20.92% of secondary palate length), large paired foramina on palatal surface of maxilla near mid-maxillary suture medial to canine, labial platform markedly concave immediately posterior to canine and less depressed posteriorly, and five sectorial postcanine teeth, with the sectorial region forming more than half of the length of the postcanine tooth row.

Etymology—Genus name derived from the isiZulu word *impi* (meaning 'combat') and the Latin word *dens* (meaning 'tooth'), in reference to the autapomorphically extensive sectorial tooth row in this taxon and its large and powerful appearance. Species named for Dr John Hancox in honor of his pioneering work on the *Cricodon-Ufudocyclops* Subzone.

DESCRIPTION

Preservation—Specimen BP/I/7976 represents the right side of the snout and palate and a portion of the right zygomatic arch of a large non-mammaliaform cynodont skull. The specimen appears largely undistorted, but exhibits some surface fractures. The anteriormost portion of the jugal is preserved but is in poor condition. The lateral surface of the snout generally is more poorly preserved than the palate, with less surface detail. The anteroventral margin of the orbit is preserved, but the skull is broken above the lacrimal, such that the nasal and prefrontal are missing. The anterior tip of the premaxilla is also missing. The ventral surface of the snout, including the secondary palate, is well preserved. All postcanine alveoli are preserved, but only the two anteriormost alveoli contain teeth. These teeth are broken off at the base of the crown, so most details of their morphology are not preserved. The canine alveolus and posterior two incisor alveoli are also preserved

without teeth. In addition to the cranial elements, there is a fractured section of rib lodged above the palatine within the snout cavity.

Premaxilla—The premaxilla is a small bone, subtriangular in ventral view, that forms the anterior tip of the snout (Fig. 1). The lateral side of its ventral surface preserves one complete and one partial alveolus for the posteriormost two incisors. The posterior margin of the premaxilla has a scarf joint where it contacts the maxilla; this suture runs posteromedially to anterolaterally, so that the posteriormost incisor alveolus is slightly overlapped laterally by the premaxilla. Posterior to this alveolus, the premaxilla forms the anterior wall of the paracanine fossa. The paracanine fossa is extremely large (32 mm in anteroposterior length by 21 mm in mediolateral width), nearly equal in size to the upper canine alveolus and situated anteromedial to it. The premaxillary and maxillary contributions to the paracanine fossa are approximately equal, with the suture between them at the midpoint of the floor of the fossa. The premaxilla makes the shortest contribution to the secondary palate of its three component bones (25 mm along the midline from its suture with the maxilla to the posterior edge of the incisor alveoli, vs. 80 mm of maxilla and 35 mm palatine). Unfortunately, its ventral surface is partially eroded, obscuring the morphology of the incisive foramina. The premaxillary contribution to the anterolateral snout surface is also poorly preserved, although a dorsal suture with the septomaxilla is visible (Fig. 2).

Septomaxilla—The septomaxilla is a small bone with a smooth dorsal surface that is subrectangular in dorsal view (Fig. 2). It includes a right-triangular projection medial to the rostrum. It is situated anterodorsal to the premaxilla in a lap joint and forms the ventral border of the unpreserved external nares. The bone is transversely wide and articulates anteriorly with the premaxilla and posteriorly with the maxilla.

Maxilla—The maxilla is a large bone forming most of the secondary palate and lateral snout surface (Figs 1–4). It bears a single alveolus for the canine and thirteen for the postcanine teeth. The maxillary contribution to the osseous secondary palate is an anteroposteriorly elongate, subrectangular element that articulates with the premaxilla anteriorly in a scarf joint and in a rounded zigzag pattern palatally. It articulates with the palatine posteriorly in a bridle joint (Fig. 1). The ventral surface of the maxillary secondary palate is slightly concave. The anteromedial portion of the palatal surface bears two oval foramina situated medial to the posterior margin of the canine, near the mid-maxillary suture. The maxillary-palatine suture is sinuous, with a short anterior process of the palatine immediately medial to the posterior palatal foramen, medial to the alveolus for PC7. The postcanine alveolar row is medially inset, with a marked labial platform lateral to the tooth row. This platform is characteristic of most trirachodontids (with the exception of *Langbergia*; Abdala et al., 2006) and traversodontids and helps to distinguish *Impidens* from more basal cynognathians such as *Cynognathus* and *Diademodon* (Liu and Abdala, 2014). This platform is prominent but relatively shallow, as in *Cricodon metabolus* (Sidor and Hopson, 2018) and differing from the more exaggerated condition of traversodontids such as *Exaeretodon* (Abdala et al., 2002). The alveolar region of the maxilla abuts the maxillary secondary palate anteriorly and palatine secondary palate, and anterior margin of the palatine, and forms a steep shelf relative to the secondary palate surface. The posterior, sectorial portion of the tooth row is broadly separated from the palatine, and there is a deep channel on the maxillary surface medial to the sectorial alveoli, continuing onto the palatine and ectopterygoid posteriorly.

The maxilla constitutes most of the lateral surface of the rostrum (Fig. 3). The sutures between the maxilla and the jugal, lacrimal, and nasal are unclear (although the preserved dorsal margin of the maxilla probably approximates the maxillary-nasal suture).

There are two opposing infraorbital foramina located at the dorsoventral mid-height on the labial platform. This condition is typical of cynognathians, being observed in, e.g., *Cynognathus crateronotus* (BP/1/4664), *Diademodon tetragonus* (BP/1/3754), *Trirachodon kannemeyeri* (BP/1/4661), *Cricodon metabolus* (Sidor and Hopson, 2018), and traversodontids such as *Exaeretodon riograndensis* (Abdala et al., 2002). An additional foramen is present posterior to the canine alveolus on the labial platform, with a smaller foramen anterodorsal to it (Fig. 3). These foramina are situated in a fossa, wherein the portion of the labial platform immediately posterior to the canine is depressed relative to the surface of the labial platform farther posteriorly. On the lateral surface of the maxilla, dorsal to this fossa, is a robust, anteroposteriorly directed ridge originating behind the canine root and extending to the base of the zygomatic arch (Fig. 3). This ridge separates the fossa on the labial platform from a second, smaller fossa on the lateral maxillary surface, also immediately posterior to the bulge of the canine root. This lateral fossa is absent in *Diademodon tetragonus* (BP/1/3754) and *Langbergia modisei* (BP/1/5362), but present in *Trirachodon berryi* (NHMUK PV R3579), *Trirachodon kannemeyeri* (BP/1/4661, BP/1/4658), and *Cricodon metabolus* (Sidor and Hopson, 2018). The maxillary contribution to the snout is dorsoventrally tall (particularly evident in the referred specimen AMNH FARB 24421, but also clearly present in the holotype; Fig. 3); comparable to the condition seen in *Cricodon metabolus* (Sidor and Hopson, 2018), *Trirachodon kannemeyeri* (AM 461), and *Cynognathus crateronotus* (BP/1/4664). *Diademodon tetragonus* (BP/1/3754) and traversodontids (e.g., *Scalenodon ribeiroae* Melo et al., 2017; *Exaeretodon riograndensis* Abdala et al., 2002) and *Langbergia modisei* (Abdala et al., 2006) have dorsoventrally lower maxillae.

Most of the medial surface of the maxilla is dorsoventrally concave (Fig. 4). This condition is especially pronounced on the anteroventral portion of the medial surface. There

is a small dorsoventrally convex area on the anterodorsal margin of the medial surface of the maxilla. Anteriorly, the medial face of the maxilla has a meandering, anterolateral-to-posteromedial suture with the premaxilla that is pierced by a large, oval foramen. Anterior to this, the maxilla has a sinuous suture with the septomaxilla, with a small posterior septomaxillary process overlying the maxilla medially. The septomaxillary foramen is above this process and contacts the septomaxillary-maxillary suture. The medial face of the snout portion of the maxilla is weakly convex, which is most evident around the canine root, where the maxilla bulges outwards both laterally and medially.

The anterior opening of the maxillary sinus is located at the posteromedial margin of the maxilla. The sinus is a deep, mediolaterally narrow recess, located approximately along the posteriormost two-fifths of the anteroposterior length of the rostrum's medial wall. The recess is formed by the medial wall and a high, thin ridge consisting anteriorly of the maxilla and posteriorly of the palatine. Along the medial wall, the lacrimal forms the posterodorsal portion of the area enclosing the recess. The portion of the sinus between the ridge and the medial wall of the rostrum is filled with matrix. The dorsalmost extent of this margin, on the lacrimal, is characterized by a prominent, anteroposteriorly extending ridge.

The maxillary canal of *Impidens* can be described two-dimensionally, as this structure shows minimal ramification along the medio-lateral axis. The maxillary canal of *Impidens* emerges from the anterior margin of the maxillary sinus (Fig. 5). As in other cynognathian cynodonts for which this structure has been figured (*Trirachodon*: Benoit et al., 2015, 2019; *Massetognathus*: Crompton et al., 2017), the maxillary canal appears shorter than in other cynodonts, since the medial alveolar canal originates from the maxillary sinus. In other non-mammaliaform cynodonts, the main trunk of the maxillary canal is longer caudally and encompasses the divergence of the medial and caudal alveolar canal (Benoit et al., 2015, 2018, 2019; Crompton et al., 2017; Pusch et al., 2019). Additionally, the medial

alveolar canal in other cynodonts branches off from the main trunk of the maxillary canal. The condition displayed by *Impidens*, *Trirachodon* and *Massetognathus*, where the medial (and caudal, where present) alveolar canal diverges from the maxillary sinus, appears unique to cynognathians among non-mammaliaform cynodonts and might be a synapomorphy for the clade (Benoit et al., 2019; Pusch et al., 2019). The caudal alveolar canal is not visible because the cranial portion preserving it was not scanned, but it most likely originated from the maxillary sinus as well, as in other cynognathians (Benoit et al., 2015, 2018, 2019; Crompton et al., 2017). At the level of the sixth postcanine tooth, the ventral portion of the maxillary sinus tapers anteriorly into a finger-like process (Fig. 5). This trait is also observed in the cynognathians *Trirachodon* and *Massetognathus*, uniquely among studied cynodonts (Benoit et al., 2015, 2019; Crompton et al., 2017). More anteriorly, at the level of the fourth postcanine tooth, the maxillary canal diverges into the external nasal canal dorsally and the rostral alveolar canal ventrally (Fig. 5). The rostral alveolar canal comprises four branches. As is usual in non-mammalian therapsids (Benoit et el., 2019), the branches of the rostral alveolar canal all terminate on the surface of the maxilla at the level of the canine socket. Dorsally, the external nasal canal is divided into two main branches (this number normally varies between two and five in non-mammalian therapsids) that are themselves divided into several smaller canals distally, ensuring the innervation and supply of most of the maxillary surface (Fig. 5). There is a small horizontal canal diverging between the roots of the external nasal and rostral alveolar canals (Fig. 5), but it is unclear to which of them this small branch belongs. As is usual in non-prozostrodontian cynodonts (Benoit et al., 2019), the anterior-most half of the maxillary canal is divided between a trifurcated branch directed anterodorsally, which represents the internal nasal canal, and one branch directed anteriorly, the superior labial canal (Fig. 5). The superior labial canal ramifies into nine smaller canals that are all oriented anteroventrally toward the ventral

margin of the maxilla (Fig. 5), and is responsible for innervating and supplying the maxilla lateral to the naris. Again, there is a small horizontal branch of unclear affinity diverging at the roots of the internal nasal ramus and superior labial rami.

Palatine—The palatine is the most posterior bone of the secondary palate and also contributes to the primary palate (Figs. 1, 2). It extends from the suture with the maxilla anteriorly to a point medial to the end of the tooth row, where it contacts the pterygoid and ectopterygoid. Its contribution to the secondary palate is a subrectangular plate terminating posteriorly in a nearly straight margin perpendicular to the long axis of the skull (Fig. 1). This is similar to the condition in *Diademodon tetragonus* (BP/1/3754) and unlike that of the secondary palate of *Trirachodon kannemeyeri* (BP/1/4658), which tapers posterolaterally. The ventral surface of the palatine in the secondary palate is weakly concave, like the maxilla. A slight, curved groove is present at the posterolateral corner of the palatine contribution to the secondary palate, medial to its suture with the maxilla. From this corner, the palatine extends posteriorly in a sharp, ventrally-directed ridge, which expands to form a part of the primary palate. Lateral to this ridge, the palatine has a narrow, triangular contribution to the sulcus medial to the sectorial tooth row. This portion of the palatine bears a small foramen anteriorly and a large, oval foramen posteriorly, at its junction with the pterygoid and ectopterygoid. Medial to the ridge, the palatine forms a backswept, 'wing'-like structure terminating in a rounded tip overlying the anterior face of the pterygoid transverse process. Anterior to this palatine 'wing' is a large cavity forming the posterior opening of the internal choana, which would have been approximately semi-circular when complete.

The maxillary-palatine articulation on the dorsal surface of the palate mirrors that of the ventral surface (Fig. 2). Posterior to this, the dorsal, internal surface of the palatine bears a sharp, transversely-oriented ridge. The dorsal portion of the palatine posterior to this ridge

forms a roughly diamond-shaped depression ventromedial to the orbit. The anterior wall of this depression features three transversely elongate fossae arranged horizontally, the dorsalmost of which is largest and the ventralmost of which probably communicates with the large ventral foramen at the junction between the palatine, pterygoid, and ectopterygoid (Fig. S3). These fossae each bear foramina, but they are somewhat obscured by matrix, making it difficult to determine their size and dimensions. Posteriorly, the dorsal surface of the palatine has a wavy suture with the pterygoid, with a laminar posterior palatine process overlapping the pterygoid surface posterolaterally.

Lacrimal—The lacrimal forms the anterior portion of the orbit and part of the lateral surface of the snout (Figs. 2–4). It contacts the palatine medially, pterygoid posteromedially, jugal ventrally, and maxilla anterolaterally, although the latter suture is not clearly visible due to poor preservation of the snout surface. The lacrimal contribution to the anterior orbital wall bears a broad fossa pierced by a large, roughly circular lacrimal foramen (Fig. S3). This foramen is the opening for the lacrimal canal, which descends anteroventrally into the maxillary sinus; it does not have an exit on the lateral snout surface. An anteroposteriorly extending ridge overlies the lacrimal canal on the medial surface of the lacrimal. Lateral to the lacrimal foramen there is a low, boss-like lacrimal eminence on the edge of the orbital margin. The anterior margin of the orbit is situated well posterior to the end of the secondary palate, as is typical of basal cynognathians such as *Diademodon tetragonus* (BP/1/3754) and *Cynognathus crateronotus* (BP/1/4664). Although the lacrimal-maxillary suture is not visible laterally, on the medial snout surface, this suture extends anterodorsally from the lateral wall of the maxillary sinus and terminates dorsally at approximately the posteriormost quarter of the anteroposterior length of the rostrum (Fig. 4). In addition to the ridge above the lacrimal canal, the medial face of the lacrimal also exhibits a tall, posterodorsally-curved process extending from its contact with the palatine ventrally.

Ectopterygoid—The ectopterygoid is an elongate, laminar bone, broadest at mid-length (Fig. 1). It is situated between the maxilla laterally and the pterygoid medially. Anteriorly, it contacts the palatine and makes a small contribution to the channel medial to the sectorial tooth row. Its anterior tip is immediately lateral to the large foramen at the junction between palatine and pterygoid; due to damage it is uncertain whether the ectopterygoid actually contributes to the margin of this foramen and it may be excluded by a thin posterior projection of the palatine. Posterolaterally, the ectopterygoid wraps around the anterior wall of the subtemporal fenestra before terminating between the lacrimal and jugal.

Pterygoid—The transverse process of the pterygoid is broken at its base, but appears to have been robust and anteroposteriorly thickened relative to the condition in *Trirachodon kannemeyeri* (BP/1/4658). The posterior face of the transverse process is curved and weakly concave, whereas anteriorly it is somewhat convex, near its contact with the palatine (Fig. 1). Laterally, the base of the transverse process curves sharply dorsally and this bone fits into a roughly triangular space with ragged edges between the ectopterygoid and lacrimal. The tip of the pterygoid does not seem to fully fit into this space, which is filled with matrix in the holotype specimen. It is uncertain whether this is due to incomplete preservation or whether this part of the pterygoid was incompletely ossified in life. Dorsal to the transverse process, the pterygoid surface is depressed, and largely confluent with the dorsal depression on the palatine (Fig. 2). This depression tapers posteromedially on the pterygoid, terminating above the anterior portion of the basicranial girder. The pterygoid is damaged posteriorly, but does form the lateral edge of the basicranial girder, presumably flanking the parabasisphenoid further posteriorly.

Dentition—The preserved alveoli include two incisors, a single canine, as well as eight gomphodont and five sectorial postcanines (Fig. 1). The preserved incisor alveoli are noticeably enlarged relative to the overall length of the tooth row, as compared to those of

most other gomphodont cynodonts, e.g., *Trirachodon kannemeyeria* (BP/1/4658), *Diademodon tetragonus* (BP/1/2522), and *Massetognathus pascuali* (BP/1/4245). This condition is similar to some gomphodontosuchine traversodontids (e.g., *Exaeretodon* spp.; MACN 18125, UFRGS PV-0808-T). The canine alveolus is also large relative to the tooth row (Table 3) and labiolingually compressed. This morphology is similar to that of *Cynognathus crateronotus* (BP/1/4664) and *Cricodon metabolus* (Sidor and Hopson, 2018). The alveolar shape of the canine tends to be more circular in *Diademodon tetragonus* (e.g.,BP/1/3754; although see Fig. 6D) and traversodontids (e.g., *Massetognathus pascuali* [Liu et al., 2008]; *Exaeretodon riograndensis* [Abdala et al., 2002]). There is effectively no diastema between the canine and the postcanine tooth row in BP/1/7976 (Table 4) and only a short diastema in AMNH FARB 24421. The absence of a diastema is shared with *Cynognathus crateronotus* (BP/1/4664) and *Langbergia modisei* (Abdala et al., 2006). This contrasts with the usual presence of short to well-developed diastemata in *Diademodon tetragonus* (BP/1/3754), *Trirachodon kannemeyeri* (BP/1/4658), and most traversodontids (e.g., *Exaeretodon riograndensis*; Abdala et al., 2002).

The gomphodont alveoli are transversely expanded and oval in occlusal view. Their labiolingual lengths and ratio between labiolingual and mesiodistal lengths increase progressively anteroposteriorly with the ratio between the labioolingual and mesiodistal dimensions of the first postcanine (gomphodont) tooth being 1.5:1, and the same ratio increasing to 2.5:1 (Table 3) in the distalmost gomphodont tooth. By contrast, the labiolingual-to-mesiodistal ratio in the distalmost gomphodont tooth of *Titanogomphodon crassus* is 1.7:1 (GSN R322) and 1.3:1 in *Diademodon tetragonus* (BP/1/3757; see also Hendrickx et al., 2019). They also lack any transitional (also called intermediate) gomphodont teeth between the gomphodont and sectorial rows (Fig. 6C, D), which are characteristic of gomphognathids (Grine, 1977; Hendrickx et al., 2019). The alveolar shape

of the gomphodont teeth in *Impidens* is more similar to those of *Trirachodon kannemeyeri* (BP/1/4658) and *Cricodon metabolus* (Sidor and Hopson, 2018) (except that the distalmost gomphodont tooth tends to be less labiolingually expanded than the preceding tooth in these taxa). However, the three gomphodont teeth preceding the distalmost in *Trirachodon kannemeyeri* (BP/1/4658), and *Cricodon* sp. (BP/1/6102) have even greater labiolingual-to-mesiodistal ratios than any of the teeth in *Impidens*, with this ratio reaching 3:1 in the penultimate gomphodont alveoli of the postcanine series in both of the latter specimens. The sectorial tooth row of *Impidens* consists of five tooth positions, a unique feature amongst gomphodont cynodonts exceeding the four sectorials present in the recently-described basal traversodontid *Etjoia* (Hendrickx et al., 2020) and some *Diademodon* specimens (Ziegler, 1969). The sectorial tooth row occupies just over half the anteroposterior length of the postcanine tooth row, a condition otherwise known only in *Etjoia* among gomphodonts. The sectorial row scribes a shallow arc in ventral view, with the anterior portion extending posterolaterally and the posterior portion becoming strictly posteriorly directed. The alveolar margin of the sectorial tooth row becomes progressively more dorsally elevated as it extends posteriorly.

PHYLOGENETIC ANALYSIS

Six most parsimonious trees of length 210 were recovered (Fig. 7, Supplementary Data 3) with a C.I. of 0.510 and an R.I. of 0.746. *Impidens hancoxi* is recovered as a trirachodontid in all trees, and Trirachodontidae is recovered as monophyletic, containing *Cricodon metabolus*, *Impidens hancoxi*, *Langbergia modisei*, *Trirachodon berryi*, and *T. kannemeyeri*. The trees differ in the relative positions of the various trirachodontid taxa. In three of the six trees, *Impidens hancoxi* is recovered as sister taxon to *Langbergia modisei*.

In two of these trees, the (*Impidens* + *Langbergia*) clade is recovered as sister taxon to all other trirachodontids. In one tree, this clade is recovered as the sister taxon to (*Trirachodon kannemeyeri* + *Cricodon metabolus*), with *Trirachodon berryi* at the base of Trirachodontidae. In two trees, *Impidens hancoxi* is recovered as sister to the clade containing *Cricodon metabolus*, *Trirachodon kannemeyeri*, and *Trirachodon berryi,* with *Langbergia modisei* at the base of Trirachodontidae. In one tree, *Impidens hancoxi* is recovered as sister taxon to *Trirachodon berryi* alone.

Trirachodontidae is supported by three synapomorphies: the presence of denticulated canines (character 40.1), three or more lower cusps in the transverse crest of the gomphodont postcanines (character 53.2), and the presence of a maxillary fossa posterior to canine root on lateral snout surface above labial platform (character 78.1). The last synapomorphy is ambiguous in some trees due to its absence in *Langbergia*. However, this character is the only one to support *Impidens* as a trirachodontid, given that the two other synapomorphies could not be scored for this species. When *Impidens* is recovered as the sister taxon of *Langbergia*, this relationship is supported by the axis of the posterior part of maxillary tooth row directed towards the center of the subtemporal fossa (character 58.1).

The relative positions of *Trirachodon berryi*, *Trirachodon kannemeyeri*, and *Cricodon metabolus* are volatile in this analysis. In the majority of trees (4) *Cricodon metabolus* and *Trirachodon kannemeyeri* are recovered as sister taxa. In two trees, we recover a monophyletic traditional *Trirachodon*, containing both *Trirachodon kannemeyeri* and *Trirachodon berryi*. Sidor and Hopson (2018) consistently recovered *Trirachodon kannemeyeri* as sister to *Cricodon metabolus* and formally referred that species to *Cricodon*. Our results suggest that this relationship is not as well supported as previously thought, and we provisionally retain the species *T. kannemeyeri* in *Trirachodon* pending further analyses

of gomphodont relationships and more detailed alpha taxonomic study of *Cynognathus* AZ cynodonts.

The results of our phylogenetic analysis are, at least partially, consistent with those of other recent analyses. Sidor and Hopson (2018) recovered a monophyletic Trirachodontidae but with equivocal results on the internal relationships of the group. Our results differ from those of Hendrickx et al. (2020), however, as this analysis failed to recover Trirachodontidae as a monophyletic group altogether. Additionally, Hendrickx et al. (2020) recovered *Titanogomphodon* as sister to *Diademodon*. In our analysis, *Titanogomphodon* is recovered as sister taxon to *Diademodon* in all MPTs, but only under some optimizations.

DISCUSSION

Impidens as a New Taxon and Referral of Antarctic Material

Impidens hancoxi is a large bodied trirachodontid characterized by a unique combination of primitive and derived gomphodont cynodont traits. It is comparable to *Diademodon*, *Titanogomphodon*, and *Etjoia* (Hendrickx et al., 2020) in the presence of a high number (i.e., >3) of sectorial teeth, but exceeds all of them in absolute number. It is comparable to *Trirachodon*, sinognathines and most traversodontids in the presence of a labial platform lateral to the tooth row. The shape of the gomphodont alveoli in *Impidens hancoxi* is similar to those of other trirachodontids, such as *Trirachodon kannemeyeri* and *Cricodon metabolus* (Crompton, 1955; Sidor and Hopson, 2018). *Impidens hancoxi* features enlarged incisors and an enlarged, labiolingually compressed canine. The latter feature is shared with *Cynognathus* (BP/1/4664), whereas both enlarged canines and incisors are seen in *Cricodon metabolus* (Sidor and Hopson, 2018). *Impidens hancoxi* is similar to

Langbergia in the high number of sectorial postcanine teeth and the direction of the axis of the posterior tooth row, which is oriented towards the medial margin of the subtemporal fenestra.

The Antarctic specimen AMNH FARB 24421 was initially mentioned by Hammer (1995; see also Hammer et al., 1990) as pertaining to a possible new genus of gomphodont. Later, in a more detailed account of the therapsid fauna of the upper Fremouw Formation, Hammer (1995) considered this specimen to be Diademodontidae *incertae sedis*, but potentially referable to the enigmatic Namibian taxon *Titanogomphodon*. AMNH FARB 24421 consists of a right snout fragment composed of almost the entirety of the maxilla, partial jugal, and partial lacrimal. The preserved maxilla is very similar to that of BP/1/7976, but comparisons of this element with that of *Titanogomphodon* are hindered by extreme dorsoventral crushing in the holotype. However, the morphology of the postcanine tooth row in AMNH FARB 24421 shows clear differences from that of *T. crassus* (Fig. 6). The tooth row of AMNH FARB 24421 is poorly preserved, but shows evidence for 12 postcanine maxillary teeth (Fig. 6B). The anteriormost four postcanines are gomphodont in form and have badly damaged crowns. The crowns of the next three more posterior postcanines are broken off, with the roots still present in the alveoli, but their proportions show that they were also gomphodont. There is a very sharp break in alveolar shape between the seventh and eighth postcanine tooth position, corresponding to the shift from gomphodont to sectorial postcanine alveoli. This closely matches the morphology of BP/1/7976 (Fig. 6A), but clearly differs from that of gomphognathids (including *Titanogomphodon*) in which there is a transitional gomphodont tooth (labiolingually less expanded than the preceding gomphodont teeth and roughly triangular/trapezoidal rather than quadrangular in outline) between the gomphodont and sectorial tooth rows (Fig. 6C, D). The sectorial tooth positions of AMNH FARB 24421 are preserved only as partial

alveoli, but five sectorial teeth can be inferred as present (based on preservation of four alveoli plus space for a fifth in the broken section of the tooth row between the second and third preserved sectorials). This combination of postcanine characters is unique to *Impidens* among cynodonts, allowing AMNH FARB 24421 to be confidently referred to that genus. The only clear difference between AMNH FARB 24421 and BP/1/7976 is the presence of a canine-postcanine diastema in the former, corresponding to the absence of the anteriormost gomphodont postcanine. However, the anterior dentition is often variable in gomphodont cynodonts and patterns frequently shift with tooth replacement (Abdala et al., 2002). As such, we do not consider this difference sufficient for specific distinction, and here refer AMNH FARB 24421 to *I. hancoxi*.

Trirachodontid Relationships

Support for Trirachodontidae in the current analysis is low. Some recent analyses of cynodont phylogeny recover Trirachodontidae as paraphyletic, with *Trirachodon* or *Cricodon* being more closely related to traversodontids than is *Langbergia* (Gaetano and Abdala, 2015; Hendrickx et al., 2020). However, a monophyletic Trirachodontidae is typically recovered in most analyses focusing on Gomphodontia (e.g., Liu and Abdala, 2014; Sidor and Hopson, 2018; Melo et al., 2017; Pavanatto et al., 2018; Schmitt et al., 2019). We also recognize a new character potentially supporting a more restrictive subclade within Trirachodontidae, namely the presence of a fossa on the lateral surface of the snout. However, we would note that this subclade is not recovered in all most-parsimonious trees, and additional work on the phylogeny of trirachodontids is needed.

Biostratigraphical and Palaeobiogeographical Implications

Comparisons between the tetrapod faunal composition of the *Cricodon-Ufudocyclops* Subzone and broadly contemporaneous Gondwanan deposits are difficult to make due to the fauna of this subzone being relatively poorly sampled (Abdala et al., 2005). Aside from the widespread distribution of *Cynognathus* and *Diademodon*, the tetrapod fauna of the *Cricodon-Ufudocyclops* Subzone is similar to that of other Anisian–Ladinian Gondwanan formations (e.g., the upper Omingonde Formation of Namibia, the upper Fremouw Formation of Antarctica, the Ntawere Formation of Zambia, and the Manda Beds of Tanzania) in broader phylogenetic terms, containing trirachodontid (and other cynognathian) cynodonts and kannemeyeriiform dicynodonts (e.g., Abdala et al., 2005; Abdala and Smith, 2009; Peecook et al., 2018; Smith et al., 2018). Surprisingly, the *Cricodon-Ufudocyclops* Subzone has yet to yield archosauromorphs, which are present in most of these other formations (e.g., Martinelli et al., 2017; Hancox et al., 2020) and from other *Cynognathus* subzones (Neveling et al., 2005; Hancox et al., 2020), suggesting that they were likely present in the region at the time of the deposition of the *Cricodon-Ufudocyclops* Subzone. The low proportional representation of traversodontid cynodonts (and complete absence of probainognathians) suggests that the *Cricodon-Ufudocyclops* Subzone is older than some other Gondwanan deposits from the Triassic where these taxa occur in greater abundance, such as the uppermost Omingonde Formation of Namibia, the upper Ntawere Formation of Zambia, the Lifua Member of the Manda Beds of Tanzania, the Chañares Formation of Argentina, and the Santa Maria Formation of Brazil (Abdala et al., 2020). These deposits also contain a higher diversity of derived archosauromorphs than their immediately older counterparts.

The shared presence of *Impidens hancoxi* between the *Cricodon-Ufudocyclops* Subzone and the upper Fremouw Formation, in conjunction with the shared presence of *Cynognathus* and absence of traversodontids (Sidor et al., 2014), strongly suggests these

deposits are time correlative. With the caveat that both strata are poorly sampled, this indicates a strong similarity between the tetrapod fauna of the early Middle Triassic of these regions. Previous research (e.g.,Abdala et al., 2005; Hancox et al., 2013) indicated the tetrapod fauna of the *Cricodon-Ufudocyclops* Subzone to be more comparable to that of the lower Manda Beds. This hypothesis was based on these strata sharing *Cricodon metabolus* and the dicynodont *Angonisaurus*, but these records have recently been questioned or refuted (Kammerer et al., 2019). Kammerer et al. (2019; see also Smith et al., 2020) regarded the identification of *Angonisaurus* in Antarctica to be tentative owing to the fragmentary nature of the referred specimen. With the addition of *Impidens hancoxi*, the composition of the tetrapod fauna of the *Cricodon-Ufudocyclops* Subzone seems to more closely resemble the fauna of the upper Fremouw Formation than of the Manda Beds.

A possible explanation of the faunal similarity between the *Cricodon-Ufudocyclops* Subzone and the upper Fremouw is that both were at a high palaeolatitude relative to other penecontemporaneous Gondwanan deposits discussed here (e.g., Martinelli et al., 2017). The area in which BP/1/7976 was found was, at the time of deposition, located at a palaeolatitude of approximately 58° south, whereas the Chañares Formation of Argentina, for example, would have been approximately 10° closer to the equator (van Hinsbergen et al., 2015). This may indicate a shared fauna between the *Cricodon-Ufudocyclops* Subzone and the upper Fremouw Formation based on adaptation to latitudinal or climatic biodiversity barriers rather than diachronous deposition from other *Cynognathus*-bearing faunas.

Palaeobiological and Palaeoecological Implications

Although it is difficult to accurately determine body mass owing to the lack of preserved limb bones and teeth, *Impidens hancoxi* is clearly among the largest known Triassic cynodonts (>400 mm total skull length). Based on the proportions of other

gomphodont crania, the complete BSL of BP/1/7976 would likely have been well over 400 mm (Tables S1 and S2). This is larger than any known complete skulls of other large cynognathian taxa, such as *Diademodon tetragonus* (e.g., BSL of 287 mm; BP/1/2522; Bradu and Grine, 1979), *Cynognathus crateronotus* (e.g., BSL of 324 mm; SAM-PK-K11484), and at least as large as *Exaeretodon argentinus* (e.g., BSL of 400 mm; MCZ 4486; Abdala et al., 2002). Keyser (1973) estimated *Titanogomphodon crassus* to have a skull length of 430 mm, though it is unclear how this conclusion was drawn. Martinelli et al. (2009) provided a slightly lower estimate of 400 mm for the reconstructed skull length of the holotype of *T. crassus* (GSN R322). *Scalenodontoides macrodontes*, a Norian traversodontid from the overlying Elliot Formation in Lesotho and South Africa, has a recorded maximum skull length of 248 mm (MNHN 1957.25; Battail, 2005). However, an incomplete snout refereable to *S. macrodontes* (NMQR 3053) has a mediolateral width of 221mm across the premaxillae. Reconstructed to MNHN 1957.25's proportions, it would have a complete skull length of 617 mm, which would make *Scalenodontoides* the largest known non-mammaliaform cynodont by a substantial margin.

The comparatively large size of *Impidens* reflects a broader trend of increased body size in cynodonts observed in the Middle Triassic (Abdala and Ribeiro, 2010). Abdala et al. (2005) suggested that trirachodontids in the *Cricodon-Ufudocyclops* Subzone and *Cricodon* in the contemporaneous Manda Beds were larger in size than specimens of other trirachodontid species (typical examples being, e.g., BSL of 100 mm for *Trirachodon berryi* [NMQR 1399] and 113 mm for *Langbergia modisei* [BP/1/5362]; Abdala et al., 2006). The holotype of *I. hancoxi* is substantially larger still than other relatively complete specimens of trirachodontids from this subzone (e.g., BP/1/5540, a *Cricodon-Ufudocyclops* Subzone specimen referred to *Cricodon*, which has a BSL of only 160 mm; the fragmentary specimen BP/1/5835 would have been somewhat larger, but not nearing *Impidens* proportions; Abdala

et al., 2005). The late Anisian and early Ladinian represent a time characterized by the following trends in tetrapod body size evolution: (1) average therapsid size reaching a maximum for the Triassic before gradually declining, and (2) average carnivore body size (regardless of clade) exceeding average herbivore body size (Sookias et al., 2012).

Gow (1978) and Hendrickx et al. (2020) have suggested that trirachodontids may have practised faunivory, insectivory, or omnivory based on the presence of serrated canines and unworn postcanine tooth crowns. Most trirachodontids also possess sectorial teeth, usually inferred to be an adaptation for slicing through flesh. The high number of sectorial teeth, and their occupation of more than half the tooth row, in *Impidens hancoxi* suggests that a substantial component of its diet was composed of animal protein. The known large herbivorous faunal elements of the *Cricodon-Ufudocyclops* Subzone are *Diademodon* and *Ufudocyclops*. The large terrestrial carnivores are represented by *Impidens hancoxi* and *Cynognathus crateronotus*, with no archosauromorphs yet recovered. With *Impidens* likely outsizing *Cynognathus* (see above), it may have represented the ecosystem's apex predator. The *Cricodon-Ufudocyclops* Subzone could perhaps represent a unique late Anisian terrestrial ecosystem in which therapsids retained the primary predator role in the absence of large-bodied archosaurs. We note, however, that the sample size of fossils from the *Cricodon-Ufudocyclops* Subzone is currently very small and further fieldwork is needed to properly understand the taxonomic composition of its tetrapod fauna.

CONCLUSIONS

Impidens hancoxi is a new trirachodontid taxon from the *Cricodon-Ufudocyclops* Subzone of South Africa, and the Fremouw Formation of Antarctica. The presence of *Impidens hancoxi* in these two units provides evidence for more precise biostratigraphic

correlation between them, refuting recent studies that question such links. *Impidens hancoxi* is diagnosed by a number of features including a very large body size relative to other trirachodontids, enlarged canines and incisors, and five sectorial teeth that form the majority of the postcanine tooth row. *Impidens hancoxi* is among the largest gomphodont cynodonts yet discovered, and certainly the largest cynodont in its ecosystem. It likely was a predator, and perhaps would have filled a role that in other penecontemporaneous deposits was occupied by archosauromorphs.

ACKNOWLEDGMENTS

We thank D. Osborne, owner of the farm Thala on which BP/1/7976 and BP/1/8123 were found, and Eve and Bernhard Howe for helping us arrange access and providing logistical support. We thank all members of the 2014 and 2017 field teams: E. Bordy, D. Cashmore, M. Day, K. Dollman, E. Dunne, M. Ezcurra, P. Godoy, A. Jones, B. McPhee, J. Neenan, P. Viglietti, and R. Sookias. We thank Pepson Mukanela for his preparation work on the specimen. We thank V. Radermacher for assisting us in improving the quality of the illustrations in this paper. Funding for field work was provided by a Marie Curie Career Integration Grant (630123 to R.J.B.), the NRF African Origins Platform (98800 to J.N.C.), and by the Palaeontological Scientific Trust (J.N.C.). C.H. was supported by a Postdoctoral Fellowship from the University Research Committee (URC) of the University of the Witwatersrand and the Consejo Nacional de Investigaciones Científicas y Técnicas (CONICET; Beca Pos-doctoral CONICET Legajo 181417). The support of the DST-NRF Centre of Excellence in Palaeosciences (CoE-Pal) towards this research is hereby acknowledged (for their role in funding F.B.T.). Opinions expressed and conclusions arrived at, are those of the author and are not necessarily to be attributed to the CoE. F.B.T. also

received funding from The PALAEONTOLOGICAL Scientific Trust (PAST), Johannesburg, South Africa.

LITERATURE CITED

Abdala, F., and L. C. Gaetano. 2018. The Late Triassic record of cynodonts: time of innovations in the mammalian lineage; pp. 407–445 in L. Tanner (ed.) The Late Triassic world. Topics in Geobiology, Volume 4. Springer, Cham.

Abdala, F., and N. P. Giannini. 2002. Chiniquodontid cynodonts: systematic and morphometric considerations. Palaeontology 45(6):1151–1170.

Abdala, F., and A. M. Ribeiro. 2010. Distribution and diversity patterns of Triassic cynodonts (Therapsida, Cynodontia) in Gondwana. Palaeogeography, Palaeoclimatology, Palaeoecology, 286(3):202–217.

Abdala, F., and R. M. Smith. 2009. A Middle Triassic cynodont fauna from Namibia and its implications for the biogeography of Gondwana. Journal of Vertebrate Paleontology 29(3):837–851.

Abdala, F., M. C., Barberena, and J. Dornelles. 2002. A new species of the traversodontid cynodont *Exaeretodon* from the Santa Maria Formation (Middle/Late Triassic) of southern Brazil. Journal of Vertebrate Paleontology, 22(2):313–325.

Abdala, F., J. C. Cisneros, and R. M. Smith. 2006. Faunal aggregation in the Early Triassic Karoo Basin: earliest evidence of shelter-sharing behavior among tetrapods? Palaios, 21(5):507–512.

Abdala, F., P. J. Hancox, and J. Nevelling. 2005. Cynodonts from the Uppermost Burgersdorp Formation, South Africa, and their bearing on the biostratigraphy and

correlation of the Triassic *Cynognathus* Assemblage Zone. Journal of Vertebrate Paleontology 25(1):192–199.

Abdala, F., L. C. Gaetano, A. G. Martinelli, M. B. Soares, P. J. Hancox, and B. S. Rubidge. 2020. Non-mammaliaform cynodonts from western Gondwana and the significance of Argentinean forms in enhancing understanding of the group. Journal of South American Earth Sciences 104. 102884.

Abdel-Kader, T. G., R. S. Ali, and N. M. Ibrahim. 2011. The cranial nerves of *Mabuya quinquetaeniata* III: Nervus Trigeminus. Life Science Journal 8:650–669.

Angielczyk, K. D., and C. F. Kammerer, C. F. 2018. Non-mammalian synapsids: the deep roots of the mammalian family tree; pp. 117–198 in F. E. Zachos, and R. J. Asher (eds.) Handbook of Zoology: Mammalia: Mammalian Evolution, Diversity and Systematics. Berlin, De Gruyter.

Battail, B. 2005. Late Triassic traversodontids (Synapsida: Cynodontia) in southern Africa. Palaeontologia africana 41:67–80.

Bellairs, A. D'A. (1949) Observations on the snout of *Varanus*, and a comparison with that of other lizards and snakes. Journal of Anatomy 83:116–146.

Benoit, J., F. Abdala., M. J. Van den Brandt, P. R. Manger, and B. S. Rubidge. 2015. Physiological implications of the abnormal absence of the parietal foramen in a late Permian cynodont (Therapsida). The Science of Nature 102(11–12):1–4.

Benoit J., K. D. Angielczyk, J. A. Miyamae, P. R. Manger, V. Fernandez, and B. S. Rubidge. 2018. Evolution of facial innervation in anomodont therapsids (Synapsida): Insights from X-ray computerized microtomography. Journal of Morphology 279(5): 673–701.

Benoit J., I. Ruf, J. A. Miyamae, V. Fernandez, P. G. Rodrigues, and B. S. Rubidge. 2019. The evolution of the maxillary canal in Probainognathia (Cynodontia, Synapsida):

Reassessment of the homology of the infraorbital foramen in mammalian ancestors. Journal of Mammalian Evolution 3:329–348.

Bordy, E. M., L. Sciscio, F. Abdala, B. W. McPhee, and J. N Choiniere. 2017. First Lower Jurassic vertebrate burrow from southern Africa (upper Elliot Formation, Karoo Basin, South Africa). Palaeogeography, Palaeoclimatology, Palaeoecology 468: 362–372.

Bradu, D. and F. E. Grine. 1979. Multivariate analysis of Diademodontine crania from South Africa and Zambia. South African Journal of Science 75:441–448.

Broom, R. 1905. On the use of the term Anomodontia. Records of the Albany Museum 1:266–269

Broom, R. 1907. On some new fossil reptiles from the Karroo beds of Victoria West, South Africa. Transactions of the South African Philosophical Society 18(1):31–42.

Crompton, A. W. 1955. On some Triassic cynodonts from Tanganyika. Proceedings of the Zoological Society of London 125:617–669.

Crompton, A.W., T. Owerkowicz, B.-A. Bhullar, and C. Musinsky. 2017. Structure of the nasal region of non-mammalian cynodonts and mammaliaforms: speculations on the evolution of mammalian endothermy. Journal of Vertebrate Paleontology 37(1).

Damiani, R. J., and P. J. Hancox. 2003. New mastodonsaurid temnospondyls from the *Cynognathus* Assemblage Zone (upper Beaufort Group; Karoo Basin) of South Africa. Journal of Vertebrate Paleontology 23(1):54–66.

Düring von, M. and M. R. Miller. 1979. Sensory nerve endings of the skin and deeper structures; pp. 407–441 in C. Gans, R. G. Northcutt, P. Ulinski (Eds.) Biology of the Reptilia Volume 9, Neurology. New-York: Academic Press.

Fire, A. 1995. 7.1. 1. FEI Visualization Sciences Group (VSG), SAS, Konrad-Zuse-Zentrum, Berlin (ZIB), 2013, 1990–2013.

Gaetano, L. C., and F. Abdala. 2015. The stapes of gomphodont cynodonts: insights into the middle ear structure of non-mammaliaform cynodonts. PloS one 10(7).

Gao, K. Q., R. C. Fox, C. F. Zhou, and D. Q. Li. 2010. A new nonmammalian eucynodont (Synapsida: Therapsida) from the Triassic of northern Gansu Province, China, and its biostratigraphic and biogeographic implications. American Museum Novitates 2010(3685):1–25.

Godefroit, P. 1999. New traversodontid (Therapsida: Cynodontia) teeth from the Upper Triassic of Habay-la-Vieille (southern Belgium). Paläontologische Zeitschrift 73(3-4):385–394.

Godefroit, P., and B. Battail. 1997. Late Triassic cynodonts from Saint-Nicolas-de-Port (north-eastern France). Geodiversitas 19(3):567–631.

Goloboff, P. A., and S. A. Catalano. 2016. TNT version 1.5, including a full implementation of phylogenetic morphometrics. Cladistics, 32(3):221–238.

Grine, F. E. 1977. Postcanine tooth function and jaw movement in the gomphodont cynodont Diademodon (Reptilia; Therapsida). Palaeontologica africana 20:123–135.

Gow, C. E. 1978. The advent of herbivory in certain reptilian lineages during the Triassic. Palaeontologica africana 21:133–141.

Gow, C. E., and P.J. Hancox. 1993. First complete skull of the Late Triassic *Scalenodontoides* (Reptilia, Cynodontia) from southern Africa. The Nonmarine Triassic. New Mexico Museum of Natural History and Science Bulletin 3:161–168.

Hammer, W. R. 1995. New therapsids from the upper Fremouw Formation (Triassic) of Antarctica. Journal of Vertebrate Paleontology 15(1):105–112.

Hammer, W. R., J. W. Collinson, W. J. Ryan. 1990. A new Triassic vertebrate fauna from Antarctica and its depositional setting. Antarctic Science, 2(2):163–169.

Hancox, P. J. 2000. The continental Triassic of South Africa. Zentralblatt für Geologie und Paläontologie Teil I 1998(11–12):1285–1324.

Hancox, P. J., and B. S. Rubidge. 1996. The first specimen of the Mid-Triassic dicynodont *Angonisaurus* from the Karoo of South Africa: implications for the dating and biostratigraphy of the *Cynognathus* Assemblage Zone, Upper Beaufort Group. South African Journal of Science 92(8):391–392.

Hancox, P. J., K. D. Angielczyk, and B. S. Rubidge. 2013. *Angonisaurus* and *Shansiodon*, dicynodonts (Therapsida, Anomodontia) from subzone C of the *Cynognathus* Assemblage Zone (Middle Triassic) of South Africa. Journal of Vertebrate Paleontology 33(3):655–676.

Hancox, P. J., J. Neveling, and B. S. Rubidge. 2020. Biostratigraphy of the Cynognathus Assemblage Zone (Beaufort Group, Karoo Supergroup), South Africa. South African Journal of Geology 2020 123(2):217–238.

Hancox, J. M., Shishkin, B. S. Rubidge, and J. Kitching. 1995. A threefold subdivision of the *Cynognathus* Assemblage Zone (Beaufort Group, South Africa) and its palaeogeographical implications. South African Journal of Science 91:143–144.

Hendrickx, C., F. Abdala, and J. N. Choiniere. 2019. A proposed terminology for the dentition of gomphodont cynodonts and dental morphology in Diademodontidae and Trirachodontidae. PeerJ 7.

Hendrickx, C., L. C. Gaetano, J. N. Choiniere, H. Mocke, and F. Abdala. 2020. A new traversodontid cynodont with a peculiar postcanine dentition from the Middle/Late Triassic of Namibia and dental evolution in basal gomphodonts. Journal of Systematic Palaeontology 18(20):1669–1706.

Hopson, J. A. 1984. Late Triassic traversodont cynodonts from Nova Scotia and southern Africa. Palaeontologica africana 25:181–201.

Hopson, J. A. 2014. The traversodontid cynodont *Mandagomphodon hirschsoni* from the Middle Triassic of the Ruhuhu Valley, Tanzania. pp. 233–253 in C. F. Kammerer, K. D. Angielczyk, and J. Fröbisch (Eds.) Early Evolutionary History of the Synapsida. Berlin: DeGruyter.

Hopson, J. A., and J. W. Kitching. 2001. A probainognathian cynodont from South Africa and the phylogeny of nonmammalian cynodonts. Bulletin of the Museum of Comparative Zoology 156(1):5–35.

Hopson, J. A., and C. A. Sidor. 2015. A juvenile specimen of the trirachodontid cynodont *Cricodon metabolus* from the Luangwa Basin of Zambia: implications for tooth replacement in gomphodont cynodonts and for trirachodontid systematics. Journal of Vertebrate Paleontology 35(Programs and Abstracts):147.

Hopson, J. A., and Sues, H. D. 2006. A traversodont cynodont from the Middle Triassic (Ladinian) of Baden-Württemberg (Germany). Paläontologische Zeitschrift, 80(2):124–129.

Kammerer, C. F., J. J. Flynn, L. Ranivoharimanana, and A. R. Wyss. 2010. The first record of a probainognathian (Cynodontia: Chiniquodontidae) from the Triassic of Madagascar. Journal of Vertebrate Paleontology 30(6):1889–1894.

Kammerer, C. F., P. A. Viglietti, J. M. Hancox, R. J. Butler, and J. N. Choiniere. 2019. A new kannemeyeriiform dicynodont (*Ufudocyclops mukanelai*, gen. et sp. nov.) from Subzone C of the *Cynognathus* Assemblage Zone, Triassic of South Africa, with implications for biostratigraphic correlation with other African Triassic Faunas. Journal of Vertebrate Paleontology 39(2).

Kemp, T. S. 1982. Mammal-like Reptiles and the Origin of Mammals. Academic Press, London, 363 pp.

Keyser, A. W. 1973. A new Triassic vertebrate fauna from South West Africa. Palaeontologica africana 16:1–15.

Keyser, A.W., 1979. A review of the biostratigraphy of the Beaufort Group in the Karoo basin of South Africa. Geological Society of South Africa Abstract Geocongess 79:13–31.

Kitching, J. W. 1977. The distribution of the Karroo vertebrate fauna: Memoir 1, Bernard Price Institute for Palaeontological Research. University of the Witwatersrand, Johannesburg.

Kitching, J.W., 1995. Biostratigraphy of the Cynognathus Assemblage Zone in B.S. Rubidge (Ed.), Biostratigraphy of the Beaufort Group (Karoo Supergroup). SACS Biostratigraphic Series, 1, Council for Geoscience, Pretoria, 46pp.

Leitch, D. B., and K. C. Catania. 2012. Structure, innervation and response properties of integumentary sensory organs in crocodilians. Journal of Experimental Biology 215:4217–4230.

Liu, J., and Abdala, F. 2014. Phylogeny and taxonomy of the Traversodontidae; pp. 255–279 in C. F. Kammerer, K. D. Angielczyk, and J. Fröbisch (eds.) Early Evolutionary History of the Synapsida. Netherlands, Springer.

Liu, J., and P. Olsen. 2010. The phylogenetic relationships of Eucynodontia (Amniota: Synapsida). Journal of Mammalian Evolution 17(3):151–176.

Liu, J., M. B. Soares, and M. Reichel. 2008. *Massetognathus* (Cynodontia, Traversodontidae) from the Santa Maria Formation of Brazil. Revista Brasileira de Paleontologia 11(1):27–36.

Liu, J., J. Ramezani, L. Li, Q. H. Shang, G. H. Xu, Y. Y. Wang, and J. S. Yang. 2018. High-precision temporal calibration of Middle Triassic vertebrate biostratigraphy: U-Pb

zircon constraints for the *Sinokannemeyeria* Fauna and *Yonghesuchus*. Vertebrata PalAsiatica 56(1):16–24.

Maddison, W. P. and D.R. Maddison. 2017. Mesquite: a modular system for evolutionary analysis. Version 3.2

Mancuso, A. C., L. C. Gaetano, J. M. Leardi, F. Abdala, and A. B. Arcucci. 2014. The Chañares Formation: a window to a Middle Triassic tetrapod community. Lethaia 47:244–265

Martinelli, A. G., E. Eltink, Á. A. Da-Rosa, and M. C. Langer. 2017. A new cynodont from the Santa Maria formation, south Brazil, improves Late Triassic probainognathian diversity. Papers in Palaeontology 3(3):401–423.

Martinelli, A. G., M. D. L. Fuente, and F. Abdala. 2009. Diademodon tetragonus Seeley, 1894 (Therapsida: Cynodontia) in the Triassic of South America and its biostratigraphic implications. Journal of Vertebrate Paleontology, 29(3):852–862.

Melo, T. P., A. G. Martinelli, and M. B. Soares. 2017. A new gomphodont cynodont (Traversodontidae) from the Middle–Late Triassic *Dinodontosaurus* assemblage zone of the Santa Maria Supersequence, Brazil. Palaeontology 60(4):571–582.

Neveling, J., J. Hancox, J., and B. S. Rubidge. 2005. Biostratigraphy of the lower Burgersdorp Formation (Beaufort Group; Karoo Supergroup) of South Africa – implications for the stratigraphic ranges of early Triassic tetrapods. Palaeontologica africana 41:81–87.

Ottone, E. G., M. Monti, C. A. Marsicano, S. Marcelo, M. Naipauer, R. Armstrong, and A. C. Mancuso. 2014. A new Late Triassic age for the Puesto Viejo Group (San Rafael depocenter, Argentina): SHRIMP U–Pb zircon dating and biostratigraphic correlations across southern Gondwana. Journal of South American Earth Sciences 56:186–199.

Owen, R. 1861. Palaeontology, or a Systematic Summary of Extinct Animals and their Geological Relations, Second Edition. Edinburgh, Adam and Black, xvi+163 pp.

Pavanatto, A. E. B., F. A. Pretto, L. Kerber, R. T. Müller, Á. A. S. Da-Rosa, and S. Dias-da-Silva. 2018. A new Upper Triassic cynodont-bearing fossiliferous site from southern Brazil, with taphonomic remarks and description of a new traversodontid taxon. Journal of South American Earth Sciences 88:179–196.

Peecook, B. R., J. S. Steyer, N. J. Tabor, and R. M. Smith. 2018 (for 2017). Updated geology and vertebrate paleontology of the Triassic Ntawere Formation of northeastern Zambia, with special emphasis on the archosauromorphs. Journal of Vertebrate Paleontology 37(6, Supp1ement).

Pusch, L. C., C. F. Kammerer, and J. Fröbisch. 2019. Cranial anatomy of the early cynodont *Galesaurus planiceps* and the origin of mammalian endocranial characters. Journal of anatomy 234(5):592–621.

Reisz, R. R., and H. D. Sues. 2000. Herbivory in late Paleozoic and Triassic terrestrial vertebrates; pp. 9–41 in R. R. Reisz, and H. D. Sues (eds.) Evolution of herbivory in terrestrial vertebrates. Cambridge University Press.

Schmitt, M. R., A. G. Martinelli, T. P. Melo, and M. B. Soares. 2019. On the occurrence of the traversodontid *Massetognathus ochagaviae* (Synapsida, Cynodontia) in the early late Triassic *Santacruzodon* Assemblage Zone (Santa Maria Supersequence, southern Brazil): taxonomic and biostratigraphic implications. Journal of South American Earth Sciences 93:36–50.

Seeley, H. G. 1894. Research on the structure, organization, and classification of the Fossil Reptilia. Part IX, Section 3. On *Diademodon*. Philosophical Transactions of the Royal Society of London 185:1029–1041.

Sidor, C. A., and J. A. Hopson. 2018 (for 2017). *Cricodon metabolus* (Cynodontia: Gomphodontia) from the Triassic Ntawere Formation of northeastern Zambia: patterns of tooth replacement and a systematic review of the Trirachodontidae; pp. 39–64 in C. A. Sidor and S. J. Nesbitt (eds.), Vertebrate and Climatic Evolution in the Triassic Rift Basins of Tanzania and Zambia. Society of Vertebrate Paleontology Memoir 17. Journal of Vertebrate Paleontology 37(6, Supplement).

Sidor, C. A., J. S. Steyer, and R. Damiani. 2001. *Parotosuchus* (Temnospondyli: Mastodonsauridae) from the Triassic of Antarctica. Journal of Vertebrate Paleontology 27(1):32–235.

Sidor, C. A., R. M. Smith, A. K. Huttenlocker, and B. R. Peecook. 2014. New Middle Triassic tetrapods from the upper Fremouw Formation of Antarctica and their depositional setting. Journal of Vertebrate Paleontology 34(4):793–801.

Sookias, R. B., R. J. Butler, and R. B. J. Benson. 2012. Rise of dinosaurs reveals major body-size transitions are driven by passive processes of trait evolution. Proceedings of the Royal Society of London B: Biological Sciences 279(1736):2180–2187.

Smith, N. J., P. J. Makovicky, C. A. Sidor, and W. R. Hammer. 2020. A kannemeyeriiform (Synapsida: Dicynodontia) occipital plate from the Middle Triassic upper Fremouw Formation of Antarctica. Journal of Vertebrate Paleontology 40(5):e1829634.

Smith, R. M. H., C. A. Sidor, K. D. Angielczyk, S. J. Nesbitt, and N. J. Tabor. 2018 (for 2017). Taphonomy and paleoenvironments of Middle Triassic bone accumulations in the Lifua Member of the Manda Beds, Songea Group (Ruhuhu Basin), Tanzania; pp. 65–79 in C. A. Sidor and S. J. Nesbitt (eds.), Vertebrate and Climatic Evolution in the Triassic Rift Basins of Tanzania and Zambia. Society of Vertebrate Paleontology Memoir 17. Journal of Vertebrate Paleontology 37(6, Supplement).

Sues, H. D., J. A. Hopson, J. A., and N. H. Shubin. 1992. Affinities of ?*Scalenodontoides plemmyridon* Hopson, 1984 (Synapsida: Cynodontia) from the Upper Triassic of Nova Scotia. Journal of Vertebrate Paleontology 12(2):168–171.

Sues, H. D., and P. E. Olsen. 1990. Triassic vertebrates of Gondwanan aspect from the Richmond Basin of Virginia. Science, 249(4972):1020–1023.

Sues, H. D., P. E. Olsen, P. E., and J. G. Carter. 1999. A late Triassic traversodont cynodont from the Newark Supergroup of North Carolina. Journal of Vertebrate Paleontology *19*(2):351–354.

van Hinsbergen, D. J. J., L. V. de Groot, S. J. van Schaik, W. Spakman, P. K. Bijl, A. Sluijs, C. G. Langereis, and H. Brinkhuis. 2015. "A paleolatitude calculator for paleoclimate studies." PloS one 10(6).

Witmer, L. M. 1995. The extant phylogenetic bracket and the importance of reconstructing soft tissues in fossils. Functional morphology in vertebrate paleontology 1:19–33.

Wynd, B. M., B. R. Peecook, M. R. Whitney, and C. A. Sidor. 2018 (for 2017). The first occurrence of *Cynognathus* in Tanzania and Zambia, with biostratigraphic implications for the age of Triassic strata in southern Pangea; pp. 228–239 in C. A. Sidor and S. J. Nesbitt (eds.), Vertebrate and Climatic Evolution in the Triassic Rift Basins of Tanzania and Zambia. Society of Vertebrate Paleontology Memoir 17. Journal of Vertebrate Paleontology 37(6, Supplement).

Ziegler, A. C. 1969. A theoretical determination of tooth succession in the therapsid Diademodon. Journal of Paleontology 43(3):771–778.

Submitted October 24, 2020; revisions received February 09, 2021; accepted Month DD, YYYY

FIGURE CAPTIONS

FIGURE 1. Ventral view of BP/1/7976. Abbreviations: **Ect**, ectopterygoid; **Fm**, foramen; **IoF**, infraorbital foramen; **Jug**, jugal; **Mx**, maxilla; **Pal**, palatine; **PalF**, palatal foramen; **PcF**, paracanine fossa; **PMx**, premaxilla; **Pt**, pterygoid. Scale bar equals 3 cm. [planned for page width]

FIGURE 2. Dorsal view of BP/1/7976. Abbreviations: **Jug**, jugal; **Lac**, lacrimal; **Mx**, maxilla; **Pal**, palatine; **PMx**, premaxilla; **Pt**, pterygoid; **SptMx**, septomaxilla. Scale bar equals 3 cm. [planned for page width]

FIGURE 3. Lateral view of BP/1/7976. **Conc**, concavity; **Fos**, fossa; **Fm**, foramen; **Jug**, jugal; **Lac**, lacrimal; **Mx**, maxilla; **PMx**, premaxilla; **Pt**, pterygoid. Scale bar equals 3 cm. [planned for page width]

FIGURE 4. Medial view of BP/1/7976. Abbreviations: **Fm**, foramen; **Jug**, jugal; **Lac**, lacrimal; **LacCan**, lacrimal canal; **Mx**, maxilla; **MxSin**, maxillary sinus; **Pal**, palatine; **PMx**, premaxilla; **Pt**, pterygoid; **SptFm**, septomaxillary foramen; **SptMx**, septomaxilla. Scale bar equals 3 cm. [planned for page width]

FIGURE 5. 3D reconstruction of the maxillary canal (green) and sinus (pink) of BP/1/7976 in lateral view. Abbreviations: **Enc**, external nasal canal; **Inc**, internal nasal canal; **Mac**, maxillary sinus; **Mac**, medial alveolar canal; **Rac**, rostral alveolar canal; **Slc**, superior labial canal. [planned for page width]

FIGURE 6. Comparison of *Impidens* dentition with gomphognathids. Photographs of all specimens in ventral view (anterior is right) with interpretive drawings of their tooth rows. **A**, BP/1/7976 (holotype of *Impidens hancoxi*); **B**, AMNH FARB 24421 (referred Antarctic specimen of *I. hancoxi*); **C**, GSN R322 (holotype of *Titanogomphodon crassus*); **D**, BSPG 1934-VIII-19 (holotype of "*Gomphognathus haughtoni*"; =*Diademodon tetragonus*). Abbreviations: **C**, upper canine tooth; **con**, conical postcanine teeth; **gom**, gomphodont postcanine teeth; **PC**, upper postcanine teeth; **sec**, sectorial postcanine teeth; **tr**, transitional postcanine tooth. Dotted lines indicate breaks in the postcanine series between tooth morphotypes; dotted outlines of alveoli indicate incomplete preservation. Scale bar equals 1 cm. [planned for page width]

FIGURE 7. Results of phylogenetic analysis, including (**A**) the strict consensus tree; and (**B**) the relationships within Trirachodontidae in all most parsimonious trees. [planned for page width]

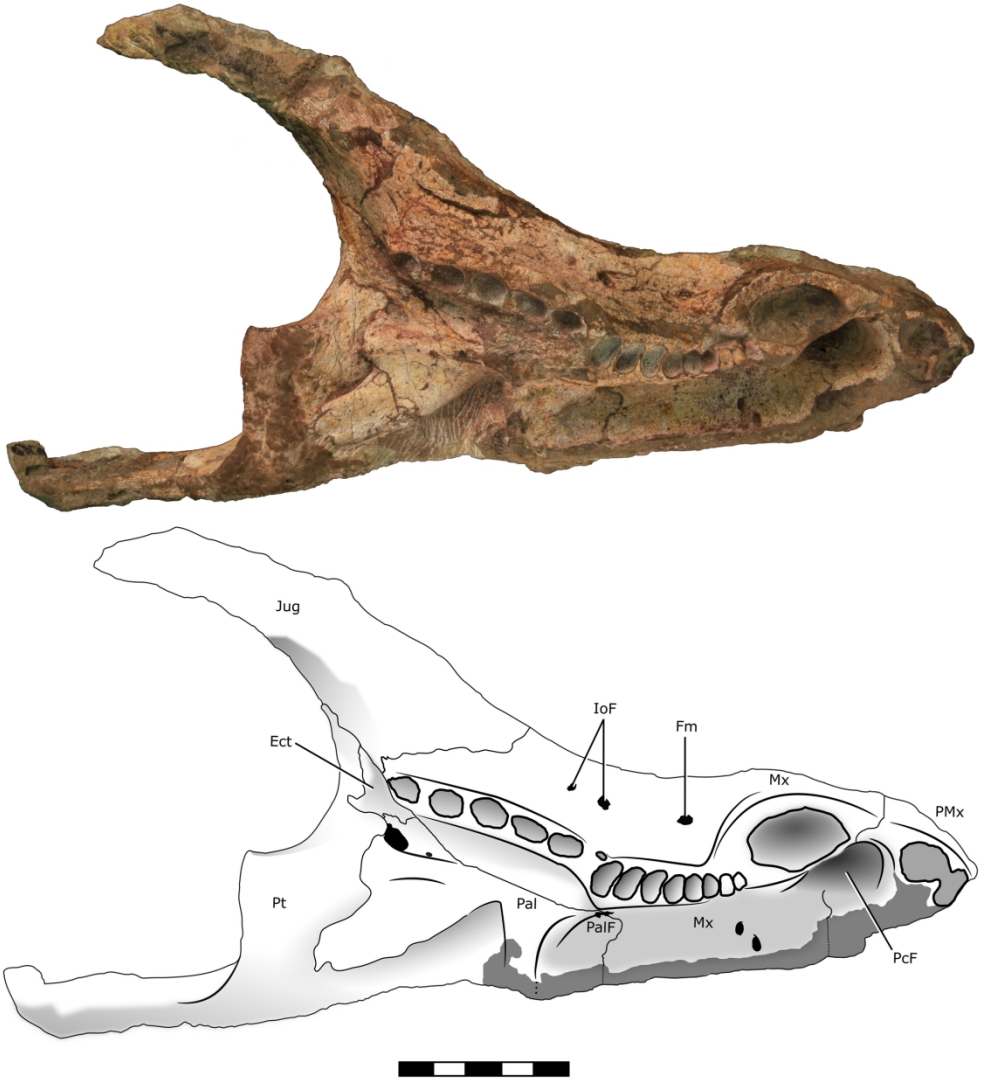

FIGURE 1. Ventral view of BP/1/7976. Abbreviations: Ect, ectopterygoid; Fm, foramen; IoF, infraorbital foramen; Jug, jugal; Mx, maxilla; Pal, palatine; PalF, palatal foramen; PcF, paracanine fossa; PMx, premaxilla; Pt, pterygoid. Scale bar = 3 cm. [planned for page width]

182x200mm (300 x 300 DPI)

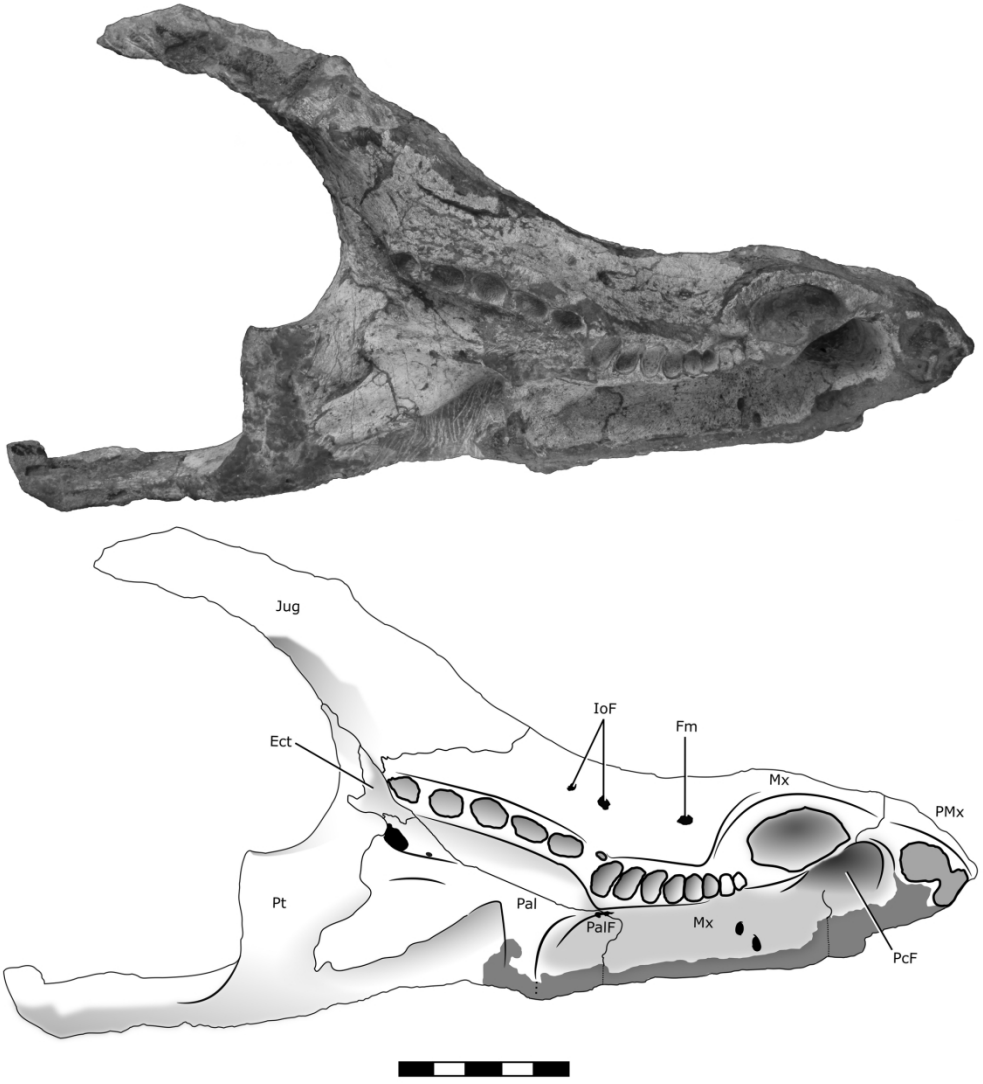

FIGURE 1. Ventral view of BP/1/7976. Abbreviations: Ect, ectopterygoid; Fm, foramen; IoF, infraorbital foramen; Jug, jugal; Mx, maxilla; Pal, palatine; PalF, palatal foramen; PcF, paracanine fossa; PMx, premaxilla; Pt, pterygoid. Scale bar = 3 cm. [planned for page width]

182x200mm (300 x 300 DPI)

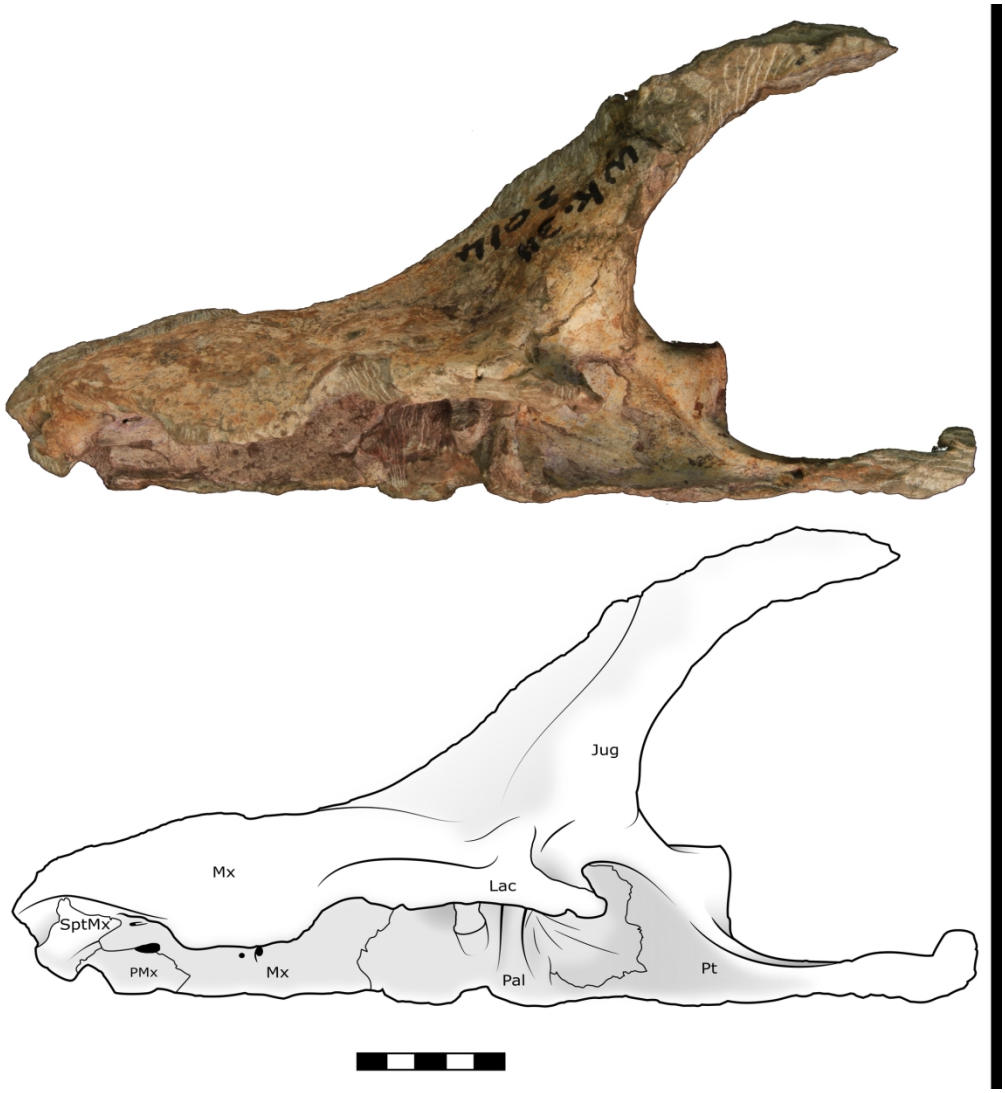

FIGURE 2. Dorsal view of BP/1/7976. Abbreviations: Jug, jugal; Lac, lacrimal; Mx, maxilla; Pal, palatine; PMx, premaxilla; Pt, pterygoid; SptMx, septomaxilla. Scale bar = 3 cm. [planned for page width]

182x198mm (300 x 300 DPI)

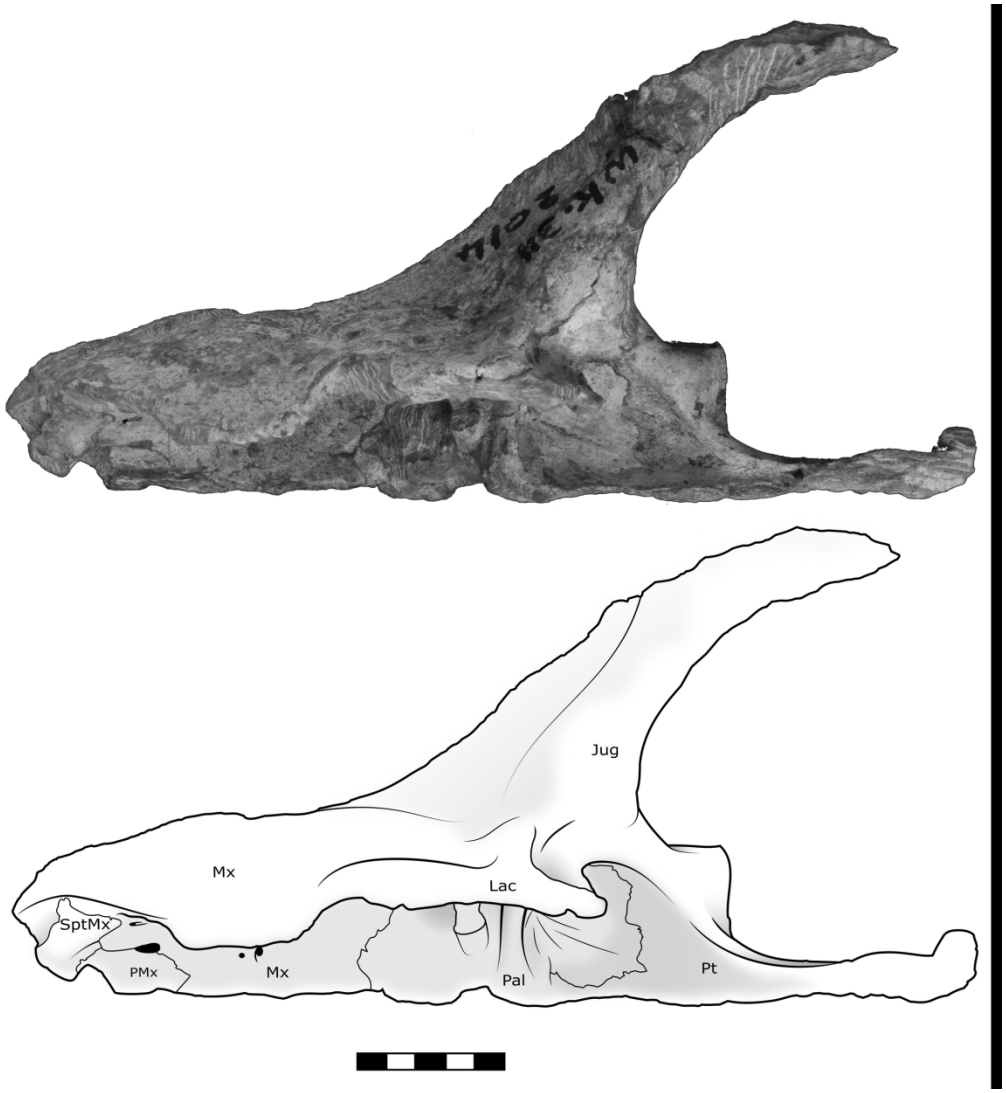

FIGURE 2. Dorsal view of BP/1/7976. Abbreviations: Jug, jugal; Lac, lacrimal; Mx, maxilla; Pal, palatine; PMx, premaxilla; Pt, pterygoid; SptMx, septomaxilla. Scale bar = 3 cm. [planned for page width]

182x198mm (300 x 300 DPI)

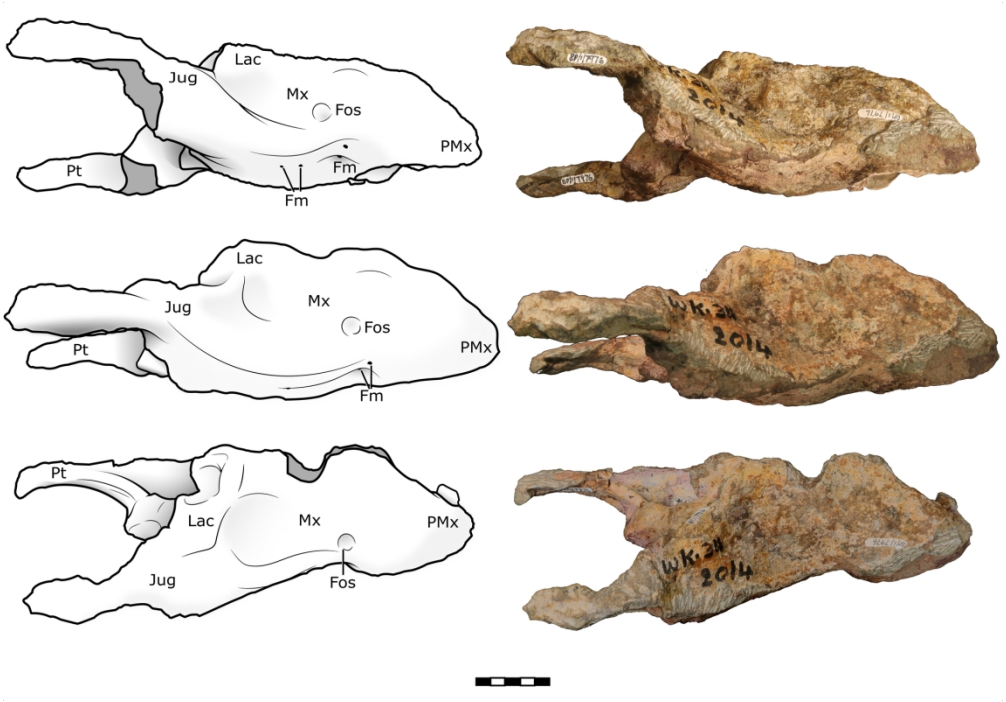

FIGURE 3. Lateral view of BP/1/7976. Conc, concavity; Fos, fossa; Fm, foramen; Jug, jugal; Lac, lacrimal; Mx, maxilla; PMx, premaxilla; Pt, pterygoid. Scale bar = 3 cm. [planned for page width]

181x127mm (300 x 300 DPI)

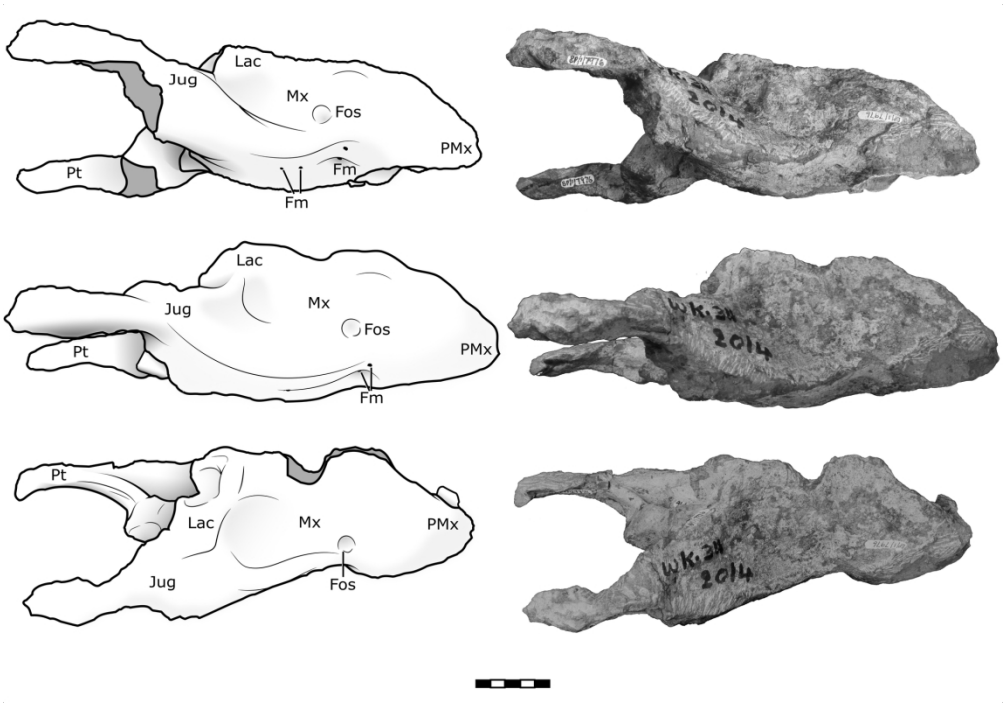

FIGURE 3. Lateral view of BP/1/7976. Conc, concavity; Fos, fossa; Fm, foramen; Jug, jugal; Lac, lacrimal; Mx, maxilla; PMx, premaxilla; Pt, pterygoid. Scale bar = 3 cm. [planned for page width]

181x127mm (300 x 300 DPI)

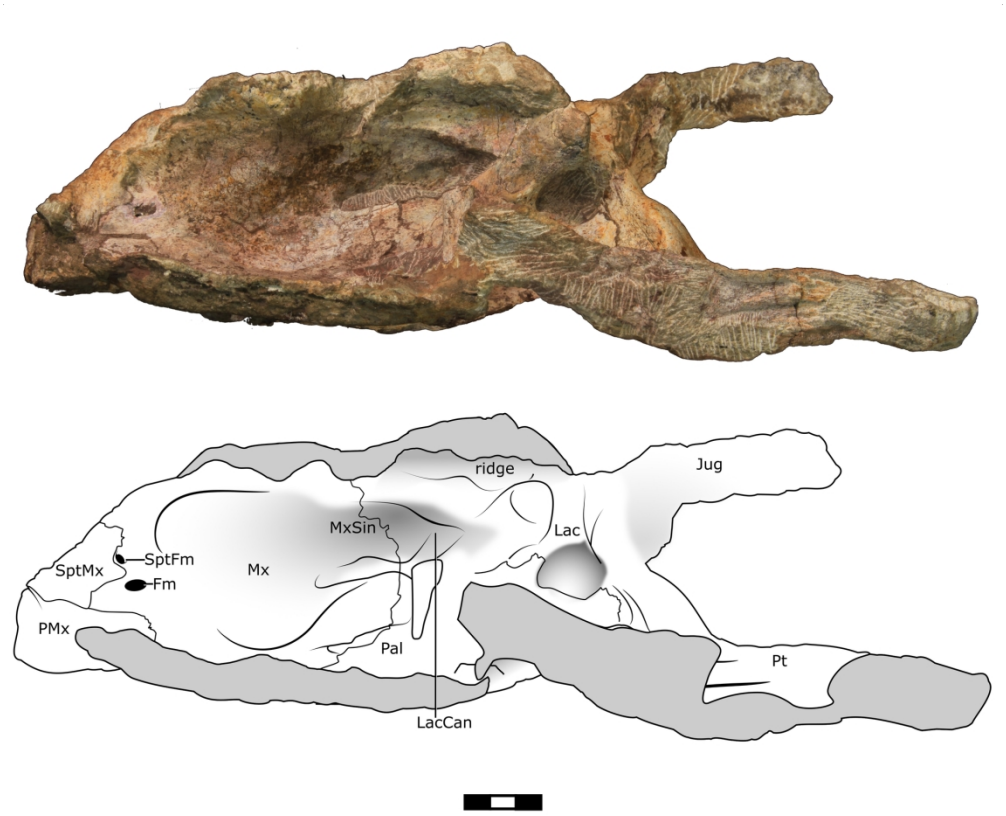

FIGURE 4. Medial view of BP/1/7976. Abbreviations: Fm, foramen; Jug, jugal; Lac, lacrimal; LacCan, lacrimal canal; Mx, maxilla; MxSin, maxillary sinus; Pal, palatine; PMx, premaxilla; Pt, pterygoid; SptFm, septomaxillary foramen; SptMx, septomaxilla. Scale bar = 3 cm. [planned for page width]

181x150mm (300 x 300 DPI)

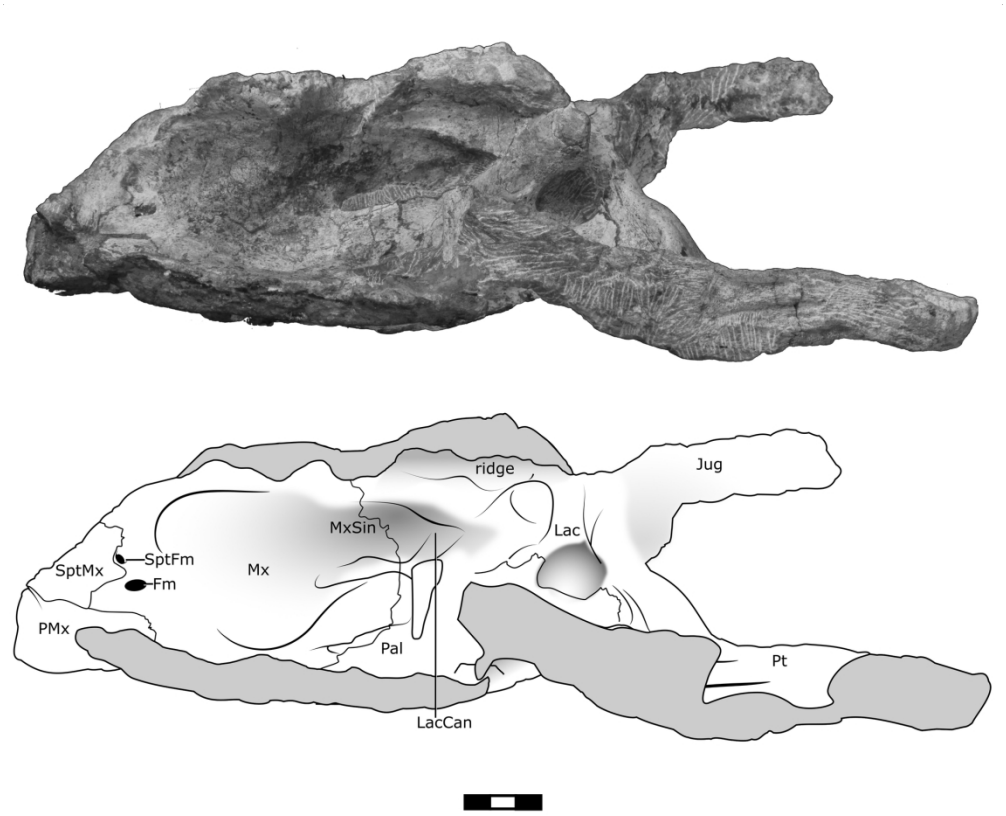

FIGURE 4. Medial view of BP/1/7976. Abbreviations: Fm, foramen; Jug, jugal; Lac, lacrimal; LacCan, lacrimal canal; Mx, maxilla; MxSin, maxillary sinus; Pal, palatine; PMx, premaxilla; Pt, pterygoid; SptFm, septomaxillary foramen; SptMx, septomaxilla. Scale bar = 3 cm. [planned for page width]

181x150mm (300 x 300 DPI)

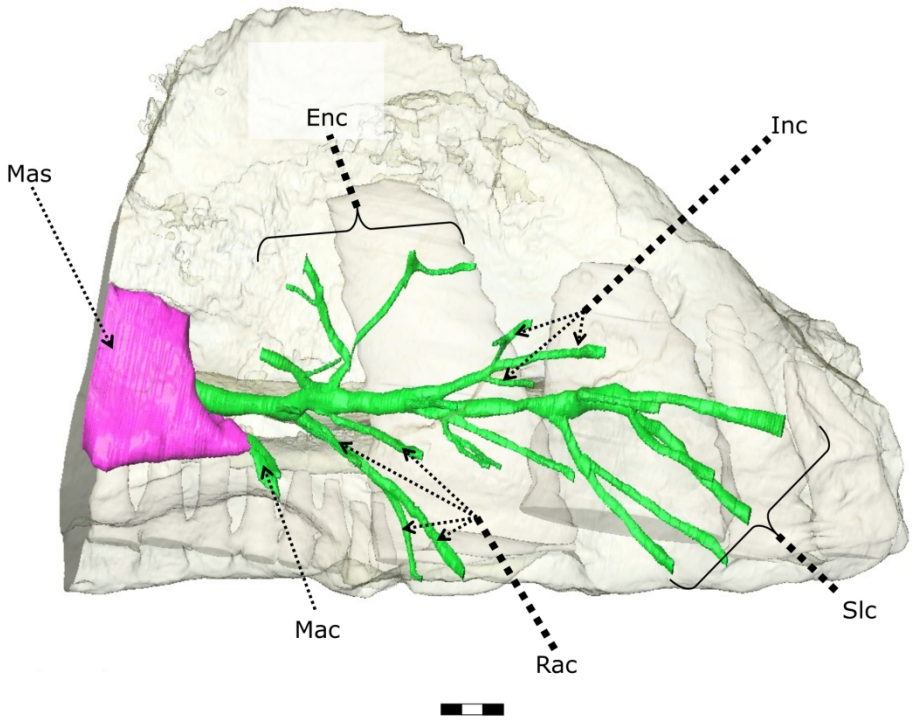

FIGURE 5. 3D reconstruction of the maxillary canal (green) and sinus (pink) of BP/1/7976 in lateral view. Abbreviations: Enc, external nasal canal; Inc, internal nasal canal; Mac, maxillary sinus; Mac, medial alveolar canal; Rac, rostral alveolar canal; Slc, superior labial canal. [planned for page width]

181x135mm (300 x 300 DPI)

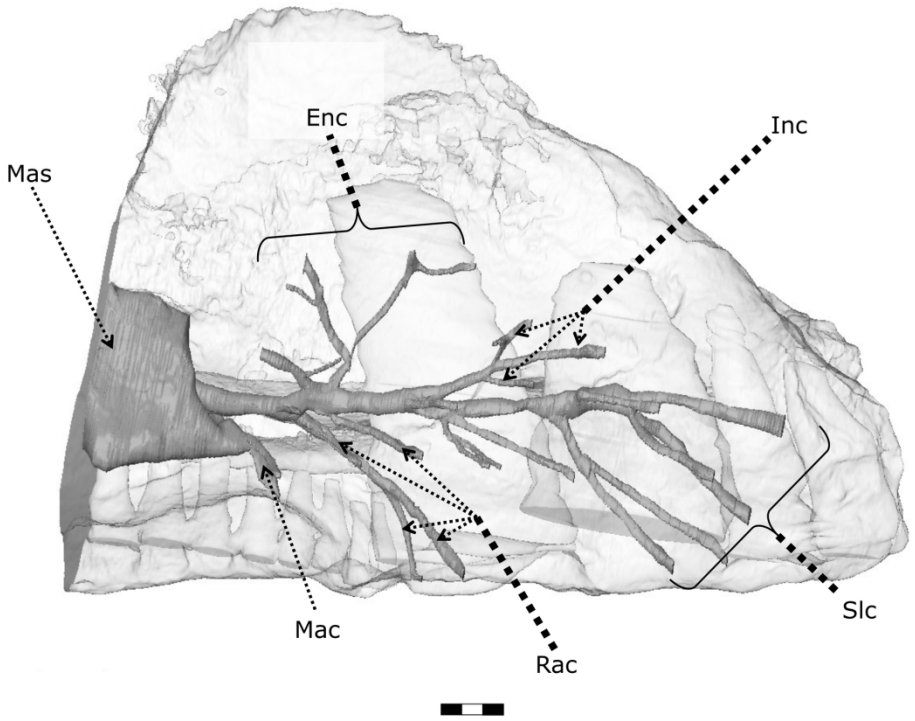

FIGURE 5. 3D reconstruction of the maxillary canal (green) and sinus (pink) of BP/1/7976 in lateral view. Abbreviations: Enc, external nasal canal; Inc, internal nasal canal; Mac, maxillary sinus; Mac, medial alveolar canal; Rac, rostral alveolar canal; Slc, superior labial canal. [planned for page width]

181x135mm (300 x 300 DPI)

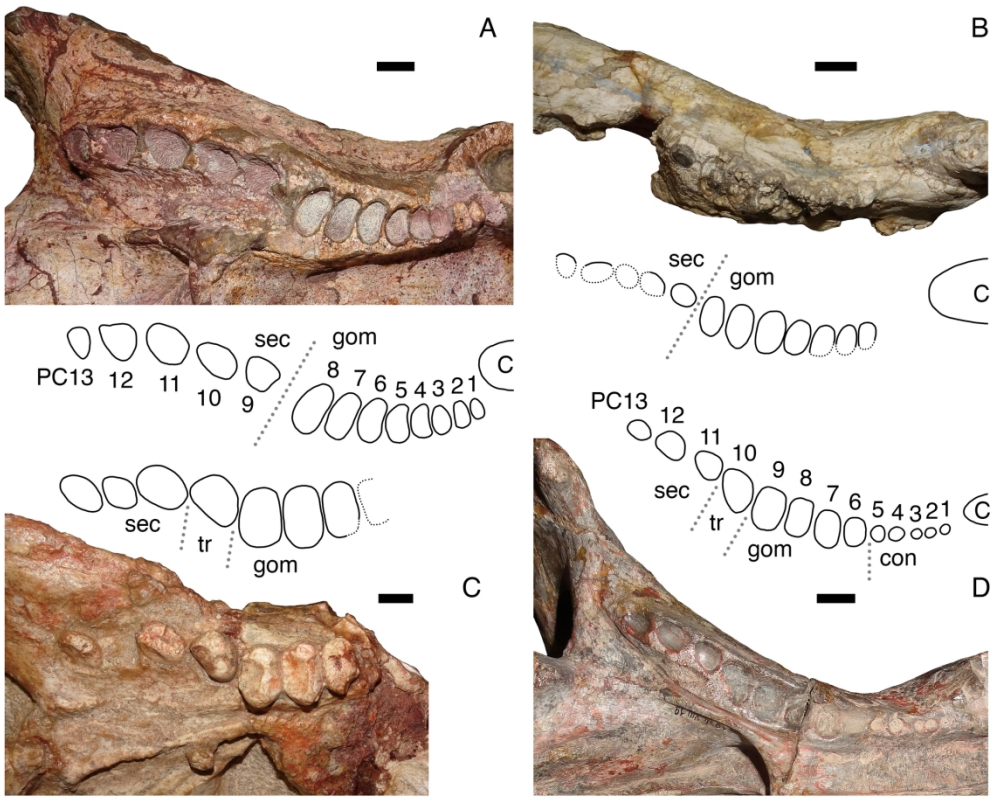

FIGURE 6. Comparison of Impidens dentition with gomphognathids. Photographs of all specimens in ventral view (anterior is right) with interpretive drawings of their tooth rows. A, BP/1/7976 (holotype of Impidens hancoxi); B, AMNH FARB 24421 (referred Antarctic specimen of I. hancoxi); C, GSN R322 (holotype of Titanogomphodon crassus); D, BSPG 1934-VIII-19 (holotype of "Gomphognathus haughtoni"; =Diademodon tetragonus). Abbreviations: C, upper canine tooth; con, conical postcanine teeth; gom, gomphodont postcanine teeth; PC, upper postcanine teeth; sec, sectorial postcanine teeth; tr, transitional postcanine tooth. Dotted lines indicate breaks in the postcanine series between tooth morphotypes; dotted outlines of alveoli indicate incomplete preservation. Scale bar equals 1 cm. [planned for page width]

182x147mm (300 x 300 DPI)

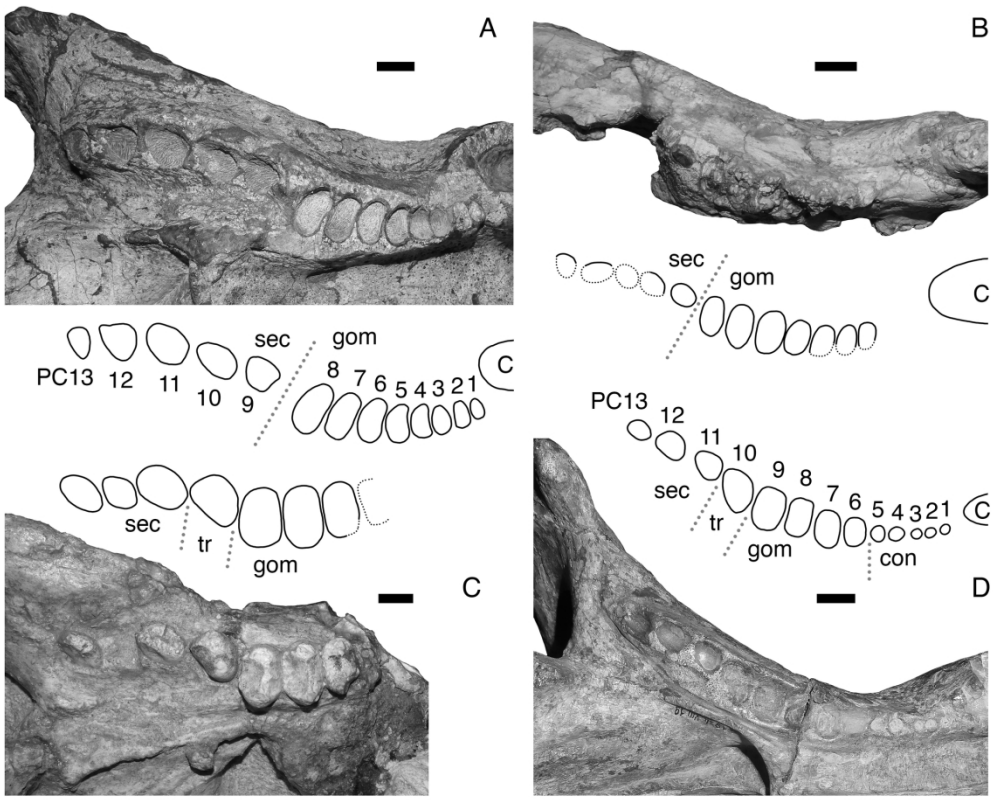

FIGURE 6. Comparison of Impidens dentition with gomphognathids. Photographs of all specimens in ventral view (anterior is right) with interpretive drawings of their tooth rows. A, BP/1/7976 (holotype of Impidens hancoxi); B, AMNH FARB 24421 (referred Antarctic specimen of I. hancoxi); C, GSN R322 (holotype of Titanogomphodon crassus); D, BSPG 1934-VIII-19 (holotype of "Gomphognathus haughtoni"; =Diademodon tetragonus). Abbreviations: C, upper canine tooth; con, conical postcanine teeth; gom, gomphodont postcanine teeth; PC, upper postcanine teeth; sec, sectorial postcanine teeth; tr, transitional postcanine tooth. Dotted lines indicate breaks in the postcanine series between tooth morphotypes; dotted outlines of alveoli indicate incomplete preservation. Scale bar equals 1 cm. [planned for page width]

182x147mm (300 x 300 DPI)

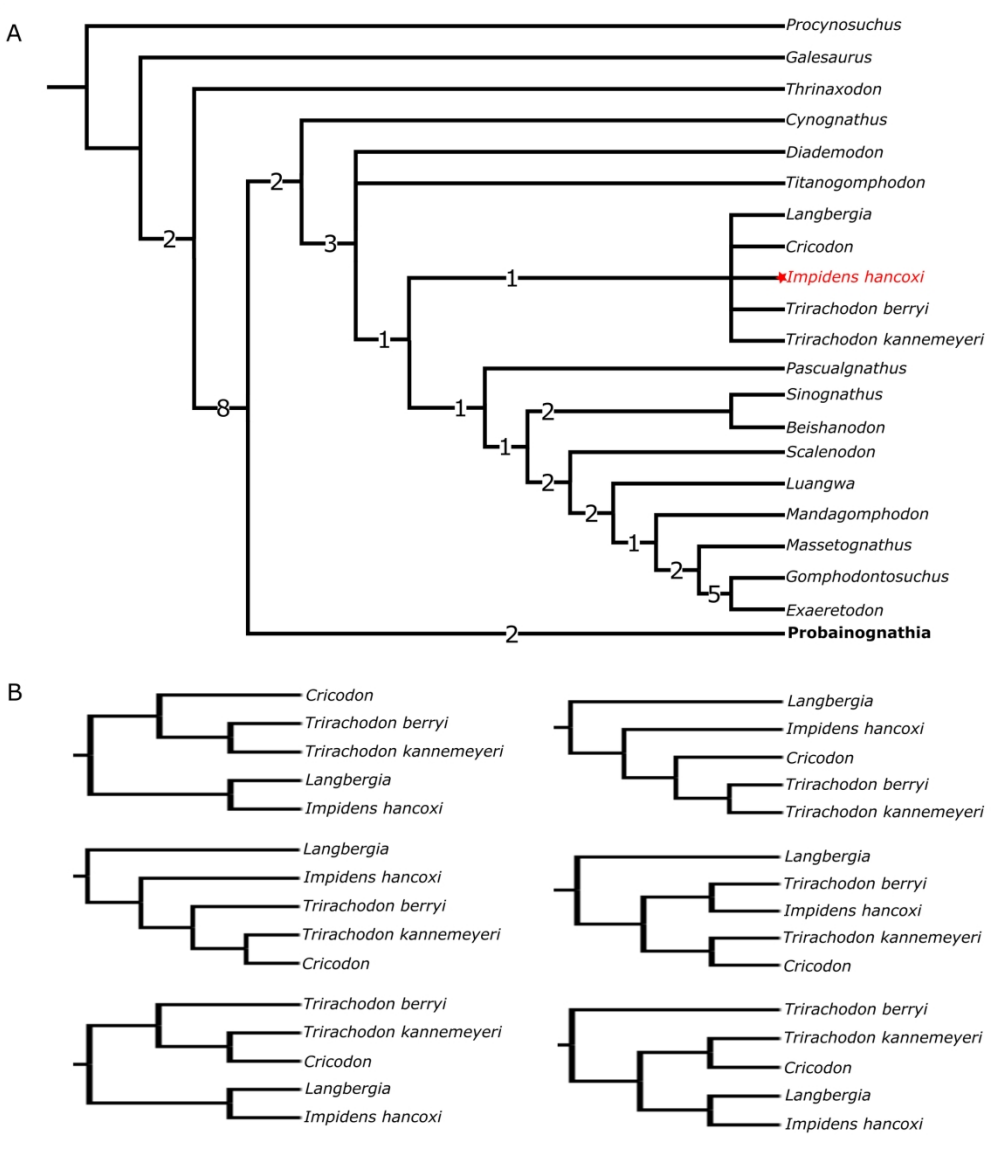

FIGURE 7. Results of phylogenetic analysis, including (A) the strict consensus tree; and (B) the relationships within Trirachodontidae in all most parsimonious trees. [planned for page width]

181x211mm (300 x 300 DPI)

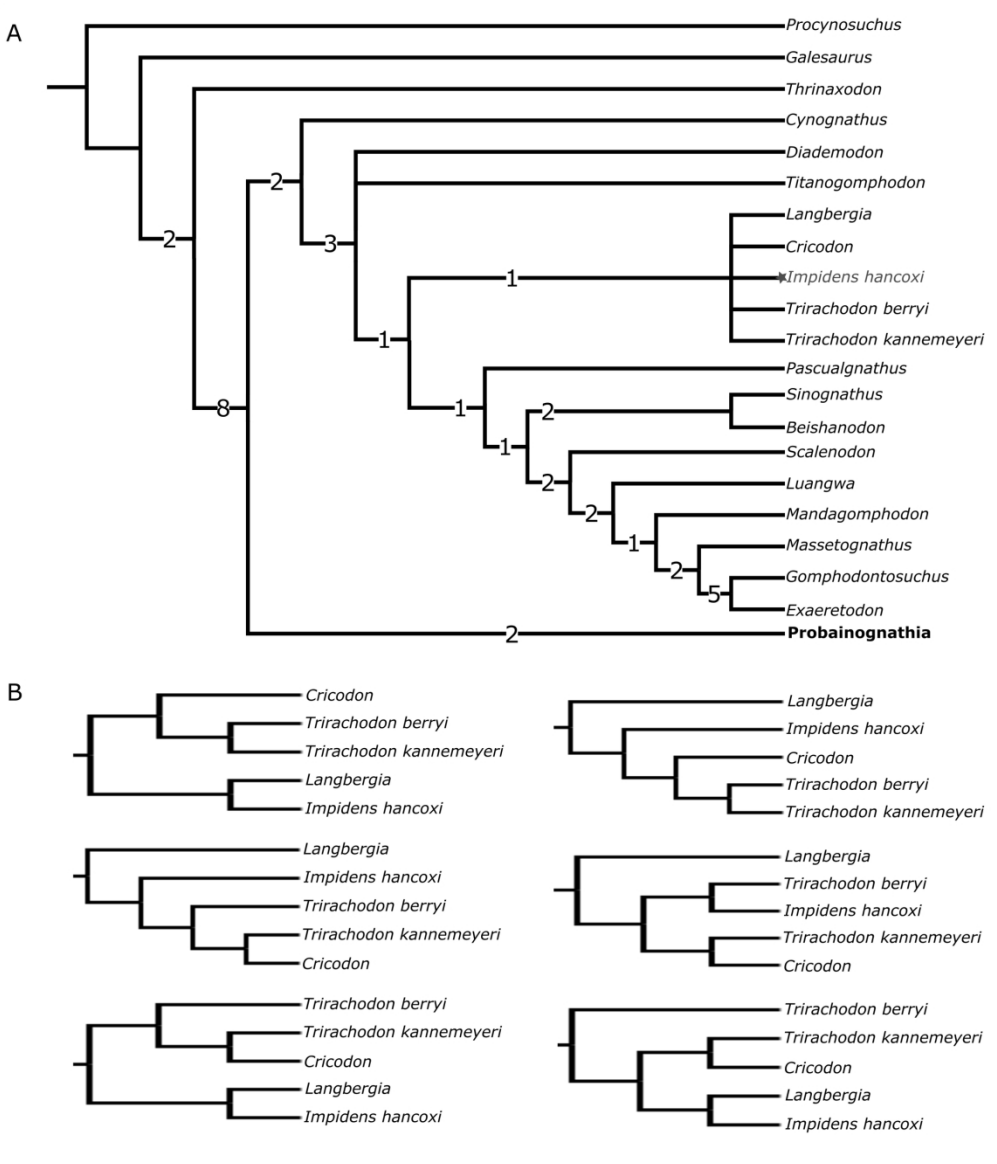

FIGURE 7. Results of phylogenetic analysis, including (A) the strict consensus tree; and (B) the relationships within Trirachodontidae in all most parsimonious trees. [planned for page width]

181x211mm (300 x 300 DPI)

TABLE 1. Cranial measurements of BP/1/7976. All lengths are measured anteroposteriorly and are in millimeters. The antorbital region is measured from the anterior tip of the snout to the anterior margin of the orbit. The secondary palate is measured from directly posterior to the first incisors to the point the osseous palate terminates posteriorly.

Antorbital region	186
Maxillary tooth row	181
Post-canine tooth row	113
Sectorial tooth row	59
Secondary	125

TABLE 2. Cynodont taxa used for comparison, along with their specimen numbers and literature sources if not seen first-hand.

Taxon	Specimen(s)	Source(s)
Cynognathus crateronotus	BP/1/4664, SAM-PK-K11484	
Diademodon tetragonus	BP/1/3772, BP/3754, BP/1/2522	
Titanogomphodon crassus	GSN R322	
Trirachodon berryi	NHMUK R3579	
Trirachodon kannemeyeri	BP/1/4661, BP/1/4658, AM 461	
Langbergia modisei	BP/1/5362, SAM-PK-11481	
"*Cricodon*" sp.	BP/1/5835	
Pascualgnathus	PVL 3466	
Massetognathus pascuali	BP/1/4245	
Massetognatus ochagaviae	UFRGS-PV0122T	Liu et al. 2008
Scalenodon angustifrons	UMZC T916	
Exaeretodon argentinus	MCZ 4486	Abdala et al. 2002
Siriusgnathus niemeyerorum	CAPPA/UFSM 0032	Pavanatto et al. 2018

TABLE 3. Dental measurements of BP/1/7976 and ratio of each alveoli's buccolingual length to its mesiodistal length. All measurements are in millimeters. Abbreviations – BL: buccolingual, MD: mesiodistal, G: gomphodont, S: sectorial.

Tooth	BL	MD	Ratio
Caniniform	14	32	0.44
G1	6	4	1.5
G2	8	5	1.6
G3	9	5	1.8
G4	10	5	2.0
G5	11	6	1.83
G6	12	6	2.0
G7	14	6	2.33
G8	15	6	2.5
S1	9	10	0.9
S2	6	12	0.5
S3	11	12	0.92
S4	9	12	0.75
S5	8	11	0.73

TABLE 4. Comparative tooth row dimensions and sectorial tooth count in some Triassic cynodonts. All measurements are in millimeters. Abbreviations: PCML: postcanine maxillary length, MD: mesiodistal/width.

Taxon	Specimen	PCML	Diastema	Canine MD	Number of sectorials
Cynognathus	BP/1/1181	103	3	25	10*
Diademodon	BP/1/3754	96	12	17	4
T. berryi	BP/1/4658	24	3	4	1
M. pascuali	BP/1/4245	31	4	4	0

SUPPLEMENTAL DATA 1

JOURNAL OF VERTEBRATE PALAEONTOLOGY

A new large gomphodont from the Triassic of South Africa and its implications for Gondwanan biostratigraphy

FREDERICK TOLCHARD,[1*] CHRISTIAN F. KAMMERER,[2,5] RICHARD J. BUTLER,[3,5] CHRISTOPHE HENDRICKX,[4,5] JULIEN BENOIT,[5] FERNANDO ABDALA,[4,5] and JONAH N. CHOINIERE[5]

[1] Evolutionary Studies Institute and School of Geosciences, University of the Witwatersrand, Johannesburg, South Africa;

[2] North Carolina Museum of Natural Sciences, 11 W. Jones Street, Raleigh, North Carolina 27601, U.S.A;

[3] School of Geography, Earth and Environmental Sciences, University of Birmingham, Edgbaston, Birmingham B15 2TT, UK;

[4] Unidad Ejecutora Lillo, CONICET-Fundación Miguel Lillo, Miguel Lillo 251, San Miguel de Tucumán 4000, Tucumán, Argentina;

[5] Evolutionary Studies Institute, University of the Witwatersrand, Johannesburg, South Africa

[*] Corresponding author.

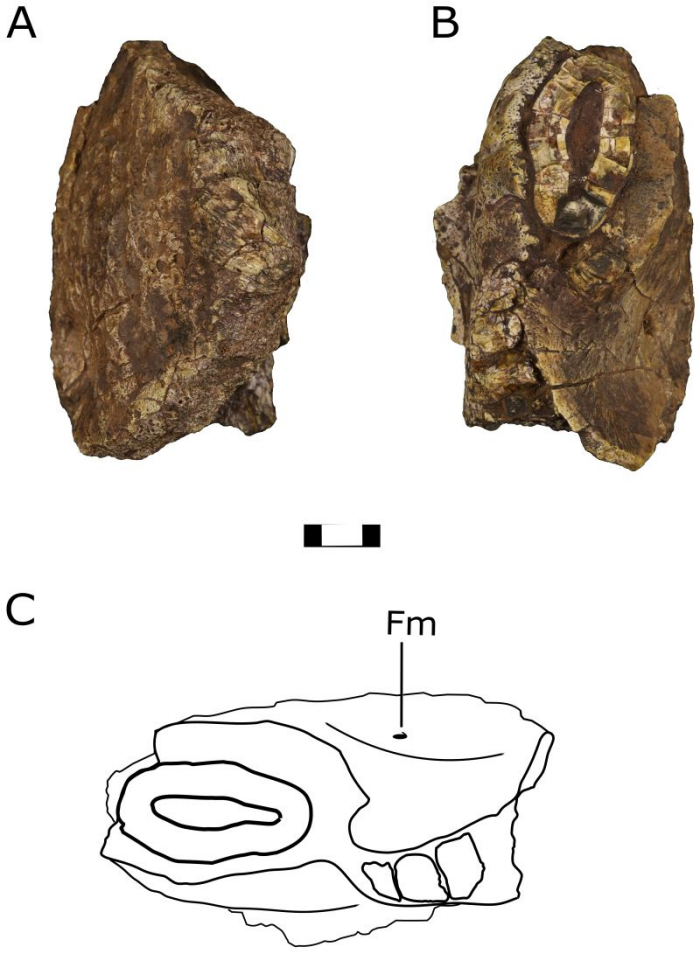

FIGURE S1: BP/1/8123, dorsal (**A**), and ventral (**B** & **C**) views. Abbreviations: **Fm**, foramen. Scale bar equals 1 cm.

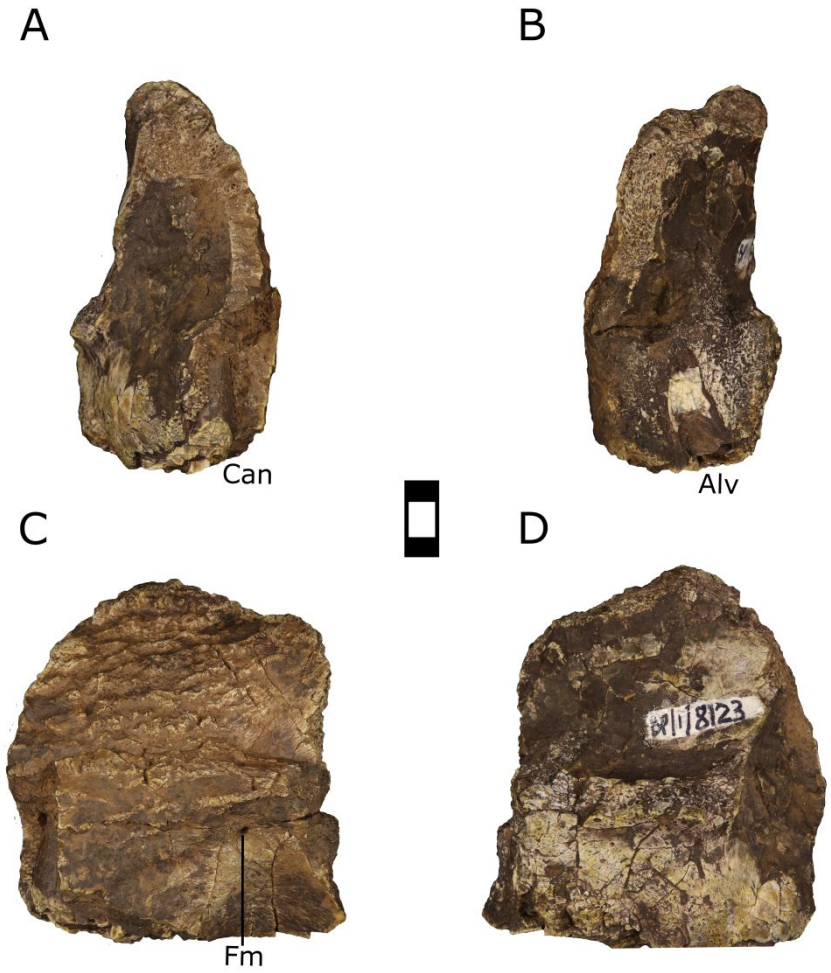

FIGURE S2: BP/1/8123 anterior (**A**), posterior (**B**), lateral (**C**), and medial (**D**) views.

Abbreviations: **Can**, canine; **Alv**, alveolus; **Fm**, foramen. Scale bar equals 1 cm.

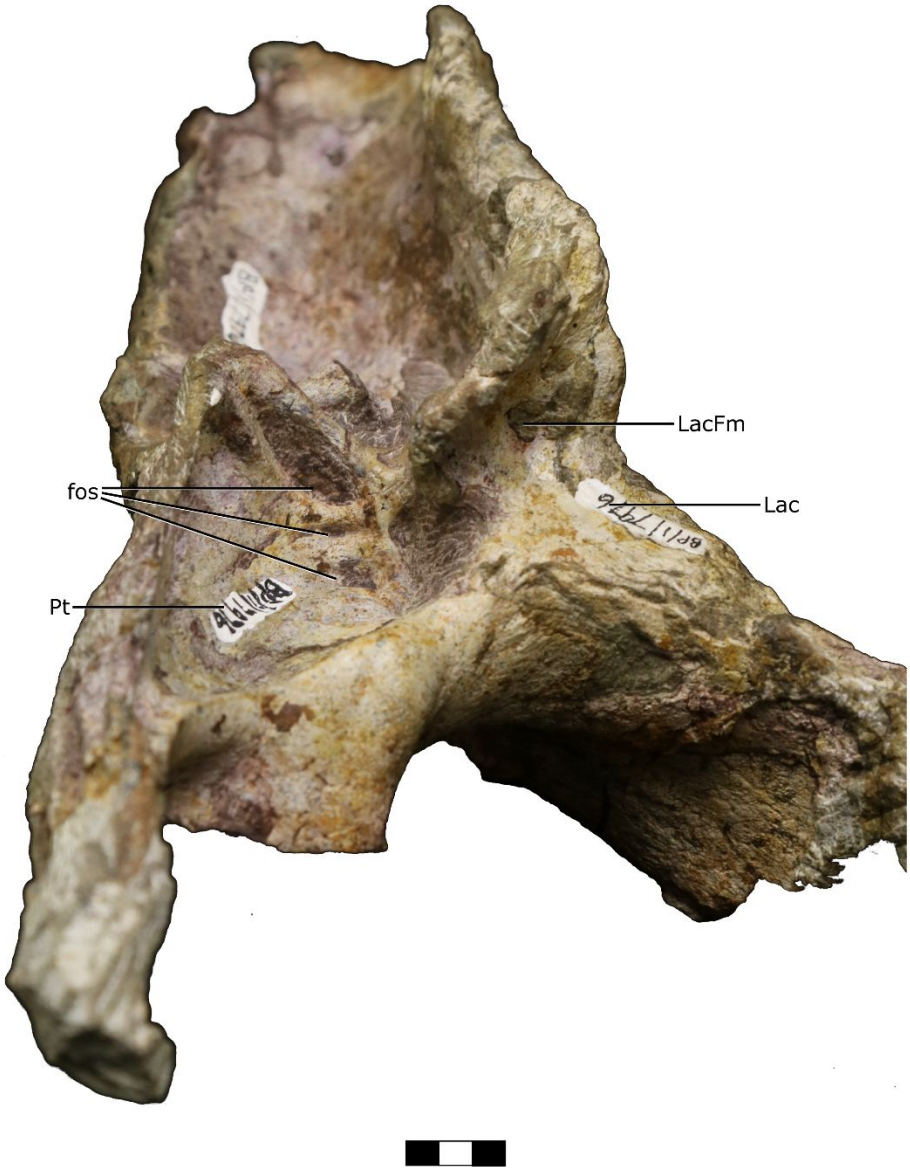

FIGURE S3: BP/1/7976, posterodorsal view. Abbreviations: **fos**, fossae; **Lac**, lacrimal; **LacFm**, lacrimal foramen; **Pt**, pterygoid. Scale bar equals 2 cm.

TABLE S1: Ratios between basal skull length (BSL) and antorbital length (AL) of various adult specimens of gomphodont cynodonts. All measurements are in millimeters.

Taxon	Specimen	BSL	AL	Ratio
Cynognathus	BP/1/4664	257	146	1.760:1
Diademodon	BP/1/3754	275	130	2.115:1
T. berryi	BP/1/4658	99	40	2.475:1
M. pascuali	BP/1/4245	88	35	2.514:1
E. riograndensis	MCP 152 PV	223	97	2.299:1

TABLE S2: The predicted BSL of BP/1/7976 based on ratios in other gomphodont cynodonts. All measurements are in millimeters.

Ratio	Predicted BSL
Cynognathus	327
Diademodon	393
T. berryi	460
M. pascuali	468
E. riograndensis	428
Total average	415
Cynognathus-Diademodon-T. berryi	394
Diademodon-T. berryi	427
Cynognathus-M. pascuali	397

APPENDIX S1. Characters 1-75 used for phylogenetic analysis are derived from Sidor & Hopson (2017). Characters 76, and 77 are taken from Liu & Abdala (2014). Character 78 is a new character. The character descriptions, state names, and codings for all taxa other than *Impidens hancoxi* are identical to those in Sidor & Hopson (2017), and Liu & Abdala 2014, with the following changes:

- Character 9: we combined States 1 and 2 because we were unable to differentiate between these states, as further elaborated on in the main text (PHYLOGENTIC ANALYSIS section).

- Character 57: *Trirachodon berryi*, *Trirachodon kannemeyeri*, and *Cricodon metabolus* changed from 2 → 1 following our reassessment of the anatomy of these taxa, as further elaborated on in the main text (PHYLOGENTIC ANALYSIS section).
- Character 59: we reworded State 1 from 'three or four' to 'three to five' to account for the five sectorial teeth present in *Impidens hancoxi*.

Characters 12, 57, 58, 59 were ordered. All characters were given equal weight.

1. Premaxilla forms posterior border incisive foramen: absent (0), present (1).

2. Position of paracanine fossa relative to upper canine: anterolingual (0), lingual (1), posterolingual (2).

3. Prefrontal: present (0), absent (1).

4. Postorbital: present (0), absent (1).

5. Parietal foramen: present (0), absent (1).

6. Vomer internarial shape: broad plate (0), parallel-sided keel (1).

7. Secondary palatal plate on maxilla: does not reach midline (0), reaches midline (1).

8. Secondary palatal plate on palatine: extends nearly to midline (0), reaches midline (1).

9. Length secondary palate relative to tooth row: shorter (0), about equal or longer (1).

10. Length secondary palate relative anterior border of orbit: shorter (0), about equal (1), longer (2).

11. Ventral surface of basisphenoid depressed below occipital condyles: less than ¼ occipital height (0), greater than ¼ occipital height (1).

12. Zygomatic arch dorsoventral height: slender (0), moderately deep (1), very deep (2).

13. Zygomatic arch dorsal extent immediately behind orbit: below middle of orbit (0), above middle of orbit (1).

14. Jugal depth in zygomatic arch relative to exposed squamosal depth: less than twice (0), greater than twice (1).

15. Jugal suborbital process: absent (0), present (1).

16. Squamosal groove for external auditory meatus: shallow (0), moderately deep (1), very deep (2).

17. Frontal-palatine contact in orbit: absent(0), present (1).

18. Descending flange of squamosal lateral to quadratojugal: absent (0), present, not contacting surangular (1), present, contacting surangular (2).

19. Internal carotid foramina in basisphenoid: present (0), absent (1).

20. Groove on prootic extending from pterygoparoccipital foramen to trigeminal foramen: present and open (0), present and enclosed as a canal (1).

21. Trigeminal nerve exit: between prootic incisure and epipterygoid (0), via foramen between prootic and epipterygoid (1), via two foramina (2).

22. Quadrate ramus of pterygoid: present (0), absent (1).

23. Greatest width of zygomatic arch: about middle of arch (anterior to level of quadrate) (0), at posterior end of arch (at level of quadrate) (1).

24. Length of palatine relative to maxilla in secondary palate: shorter (0), about equal (1), longer (2).

25. Posterolateral end of maxilla: passes obliquely posterodorsally into suborbital bar (0), forms right angle ventral to jugal contact (1).

26. V-shaped notch separating lambdoidal crest from zygomatic arch: absent (0), present (1).

27. Dentary symphysis: not fused (0), fused (1).

28. Dentary masseteric fossa: high on coronoid region (0), extends to lower border of dentary (1).

29. Dentary coronoid process height: below middle of orbit (0), above middle of orbit (1).

30. Position of dentary-surangular dorsal contact relative to postorbital bar and jaw joint: closer to postorbital bar (0), midway between (1), closer to jaw joint (2).

31. Postdentary rod height relative to exposed length (distance between base of reflected lamina and jaw joint): greater than one-half length (0), about one-half length (1), less than onehalf length (2).

32. Reflected lamina of angular posterior extent relative to distance from angle of dentary to jaw joint: greater than ½ the distance (0), less than ½ the distance (1).

33. Reflected lamina of angular shape: spoon-shaped plate (0), hook with depth greater than onehalf length (1), hook with depth less than one-half length (2).

34. Upper incisor number: five or more (0), four (1), three (2).

35. Lower incisor number: four or more (0), three (1), two (2).

36. Incisor cutting margins: smoothly ridged (0), serrated (1), denticulated (2).

37. Incisor size: all small (0), some or all enlarged (1).

38. Upper canine size: large (0), reduced in size (1), absent (2).

39. Lower canine size: large (0), reduced in size (1), absent (2).

40. Canine serrations: absent (0), present (1).

41. Upper postcanine buccal cingulum: absent (0), present (1).

42. Postcanine lingual cingulum: narrow (0), absent (1), lingually expanded (2).

43. Number of upper cusps in transverse row: one (0), two (1), three or more (2).

44. Position of upper transverse cusp row on crown: on anterior half of crown (0), from midcrown almost to posterior margin (1), at posterior margin (no posterior cingulum) (2).

45. Central cusp of upper transverse row: absent (0), about midway between buccal and lingual cusps (1), closer to lingual cusp (2).

46. Longitudinal shear surface of main upper buccal cusp: anterior and posterior (to transverse ridge, if present) (0), posterior only (1), anterior only (2).

47. Upper anterobuccal accessory cusp: present (0), absent (1).

48. Upper posterobuccal accessory cusp: present (0), absent (1).

49. Upper anterolingual accessory cusp: absent (0), present (1).

50. Upper anterior transverse (cingulum) ridge: low (0), high (1).

51. Upper lingual ridge: absent (0), present (1).

52. Transverse axis of crown strongly oblique to midline axis: absent (0), present (1).

53. Number of lower cusps in transverse row: one (0), two (1), three or more (2).

54. Lower anterior cingulum or cusp: present (0), absent (1).

55. Posterior occlusal basin on lower postcanines: absent (0), present (1).

56. Wider lower cusp in transverse row: lingual (0) buccal (1).

57. Posterior portion maxillary tooth row inset from lateral margin of maxilla (cheek developed): absent (0), moderately set in (1), well set in (2).

58. Axis of posterior part of maxillary tooth row: directed lateral to subtemporal fossa (0), directed towards center of fossa (1), directed toward medial rim of fossa (2).

59. Number of posterior sectorial postcanines: six or more (0), three to five (1), one or two (2), none (gomphodont) (3).

60. Postcanine replacement pattern in adult: “alternating” (0), widely-spaced waves (three or more teeth per wave) (1), single wave (2).

61. Expanded costal plates on ribs: absent (0), present (1).

62. Lumbar costal plates with ridge overlapping preceding rib: absent (0), present (1).

63. Acromion process: absent (0), present (1).

64. Scapular constriction below acromion: absent (0), present (1).

65. Procoracoid in glenoid: present (0), barely present or absent (1).

66. Procoracoid contact with scapula: greater than coracoid contact (0), equal to or less than coracoid contact (1).

67. Manual digit III phalanx number: four (0), three (1).

68. Manual digit IV phalanx number: four (0), three (1).

69. Length of anterior process of ilium anterior to acetabulum (relative to diameter of acetabulum): between 1.0 and 1.5 (0), greater than 1.5 (1).

70. Length of posterior process of ilium posterior to acetabulum (relative to diameter of acetabulum): between 0.5 and 1.0 (0), greater than 1.0 (1), less than 0.5 (2).

71. Dorsal profile of ilium: strongly convex (0), flat to concave (1).

72. Total length of pubis relative to acetabulum diameter: Between 1.5 and 1.0 (0), less than 1.0 (1).

73. Greater trochanter separated from femoral head by distinct notch: absent (0), present (1).

74. Lesser trochanter position: on ventromedial surface of femoral shaft (0), on medial surface of femoral shaft (1).

75. Vertebral centra: amphicoelous (0), platycoelous (1).

76. Postcanine tooth row in adults: Formed by sectorial (0), Conical, gomphodont and sectorial (1), Gomphodont and sectorial (2), Gomphodont (3).

77. Overall morphology of the upper gomphodont postcanines in occlusive view: Ovoid-ellipsoid (0), Nearly rectangular (1), Nearly triangular (2).

78. Maxillary fossa posterior to canine root on lateral snout surface above labial platform: Absent (0), Present (1).

Parsimony analysis

Characters were scored using Mesquite (Maddison & Maddison 2017). The data matrix was then exported as a .tnt file and analyzed in TNT (Goloboff & Catalano 2016) using a traditional search (TBR) with 1000 replications and one MPT saved per replication. A second round of TBR branch swapping was then conducted on the retained MPTs.

LITERATURE CITED

Goloboff, P. A., and S. A. Catalano. 2016. TNT version 1.5, including a full implementation of phylogenetic morphometrics. Cladistics, 32(3):221-238.

Liu, J., and Abdala, F. 2014. Phylogeny and taxonomy of the Traversodontidae; pp. 255-279 in C. F. Kammerer, K. D. Angielczyk, and J. Fröbisch (eds.) Early Evolutionary History of the Synapsida. Netherlands, Springer.

Maddison, W. P. & D.R. Maddison. 2017. Mesquite: a modular system for evolutionary analysis. Version 3.2

Sidor, C. A., and J. A. Hopson. 2017. *Cricodon metabolus* (Cynodontia: Gomphodontia) from the Triassic Ntawere Formation of northeastern Zambia: patterns of tooth replacement and a systematic review of the Trirachodontidae; pp. 39–64 in C. A. Sidor and S. J. Nesbitt (eds.), Vertebrate and Climatic Evolution in the Triassic Rift Basins of Tanzania and Zambia. Society of Vertebrate Paleontology Memoir 17. Journal of Vertebrate Paleontology 37(6, Supplement).